GEORGIA INSTITUTE OF TECHNOLOGY
School of Mechanical Engineering

THE INTERACTION OF A TURBULENT PIPE FLOW WITH A LONGITUDINALLY RESONANT ACOUSTIC FIELD

Final Report

National Science Foundation

Grant No. GK-5524

By

Kent C. Williams
Principal Investigator

June, 1973

GEORGIA INSTITUTE OF TECHNOLOGY
School of Mechanical Engineering

THE INTERACTION OF A TURBULENT PIPE FLOW WITH A LONGITUDINALLY RESONANT ACOUSTIC FIELD

Final Report

National Science Foundation

Grant No. GK-5524

June, 1973

Kent C. Williams
Principal Investigator

Stothe P. Kezios, Director
School of Mechanical Engineering

Table of Contents

I. Abstract

It has been found that a longitudinally resonant acoustic field, if intense enough, can affect the normal turbulence structure of flow in a horizontal circular pipe. Hot-wire anemometer measurements have shown the magnitude of the effect on the spectra of the longitudinal, radial, and circumferential turbulence components as well as the effect on the longitudinal and lateral microscale. Sound pressure levels of up to 148.5 db were employed in regard to these measurements.

In addition a qualitative description of the flow field during the interaction process was obtained employing high speed photography (2000 frames per second). A radical change in the flow field was observed and photographed when the test section was in longitudinal resonance. The qualitative description of the flow field was in agreement with earlier interpretations of similar hot-wire anemometer measurements.

Nomenclature

B	bandwidth of electronic filter
C_o	isentropic speed of sound, ft/sec
$\bar{e}^2$	mean square voltage volts^2
$\bar{e}^2_f$	mean square voltage in the bandwidth centered about the frequency f_c volts^2
$E(f)$	energy spectral density (one dimensional) Volt^2/Hz
$E(K_1)$	energy spectral density (one dimensional) Volt^2-ft
f_c	filter center frequency (Hz)
f_o	fundamental frequency of oscillation (Hz)
f_n	harmonic frequencies of the pipe (Hz)
$F(f)$	normalized energy density (one dimensional) (Hz)$^{-1}$
$F(K_1)$	normalized energy density (one dimensional) ft
f	frequency of the disturbance, Hz
H	gain of electronic filter at the center frequency
K_1	one dimensional wave number ft^{-1}
L	geometric length of the pipe, ft
L_e	effective length of the pipe, ft
n	integer
P'_{rms}	root-mean-square acoustic pressure μ bar
$P_{ref\ rms}$	reference pressure, μ bar
P'	acoustic pressure fluctuation, lbf/ft^2
r'	dimensionless distance, $r' = r/\delta ac$
r	radial location, feet
R	radius of the test section, ft
R'	dimensionless test section radius $R' = \frac{R}{\delta ac}$
$R(x)$	longitudinal correlation function

$R(\tau)$	auto correlation function
SPL	sound pressure level, db
t	time, sec
t'	dimensionless time, $t' = \omega t/2\pi$
u_1	acoustic particle velocity, ft/sec
U_o	amplitude of the acoustic particle velocity, ft/sec
$\overline{u^2}$	mean square longitudinal turbulent velocity ft^2/sec^2
$\overline{u^2}_f$	mean square velocity in the bandwidth centered about the frequency f_c ft^2/sec^2
$\bar{U}$	local mean velocity of the fluid ft/sec
x	axial location measured from inlet ft.
y	radial location measured from wall in.
δ_{ac}	A.C. boundary layer thickness, in.
γ	dimensionless distance, $\gamma = \omega t/2\pi$
ω	circular frequency, radians/sec
λ	wavelength of the sound disturbance, ft
λ_x	longitudinal microscale from the u' spectrum in.
λ_r	lateral microscale from the v' spectrum in.
Λ_x	longitudinal macroscale from the u' spectrum in.
ρ_o	equilibrium density, lbm/ft^3

Subscripts

u	longitudinal component
v	radial component
w	circumferential component
x	longitudinal
r	radial

o equilibrium condition

II. Introduction

The study of turbulent flows as a class has always provided a challange to the investigator trying to more fully understand both the structure of the turbulent flow field itself,as well as trying to understand the physical mechanisms involved in the associated transport processes. Because of the complexity of the mathematical problem statement in which there are four governing equations (continuity and three Reynold's equations) and ten unknowns (the time mean pressure, the three time mean velocity components, and the six unique stresses in the Reynolds stress tensor) the problem is generally attacked experimentally. There are exceptions to this in that certain type flow fields and geometric configurations lend themselves to some analytical treatment, but many practical flow fields do not fall in this catagory. Even the simplification to four equations and ten unknowns is subject to a suitable averaging process where it is assumed that the statistical and time average may be interchanged although there is no mathematical proof in fluid mechanics that this is valid.

The superposition of an oscillating longitudinal velocity component (generated acoustically) on the mean turbulent flow field adds an additional dimension to the complexity of the problem. The objective of the current study is to further the current state of the knowledge available in regard to oscillating turbulent flows where the periodic perturbation on the normal turbulent flow is generated with a longitudinally resonant acoustic field.

Interest in such an interaction phenomenon has existed for a number of years and the early interest centered around the study of the effects of resonant acoustic fields on heat transfer coefficients in isothermal

horizontal pipe flow.[1] Of primary interest is the fact that two distinct types of flow apparently exist as illustrated by the data in Figures 1 and 2. Under the conditions of longitudinal acoustic resonance, regions of maximum acoustic particle velocity (velocity antinodes) occur one half wave length apart, and one quarter wave length from a velocity antinode occurs a position of zero acoustic particle velocity called a velocity node. The wavelength (and hence the actual physical distance between velocity nodal points and antinodal points) depends on both the frequency of the acoustic excitation as well as the temperature of the fluid. The flow field in the study of Reference 1 was turbulent but not fully developed and the results of that investigation were the following: (i) the variation in the local Nusselt numbers with axial position was periodic with a period equal to one half the wavelength of the standing sound field and (ii) the maximum value of the local Nusselt number occurred at velocity nodes and was approximately equal to the no sound value, while the miminum occurred just downstream of the velocity antinodes. It is clear from Figure 1 that the local heat transfer rate at the velocity antinode was considerably reduced when compared to the no sound value at the same axial location. The data of this figure is representative of a turbulent flow condition with a Reynolds number of about 50,000 and is in striking contrast to that of Figure 2 which represents data taken at a lower Reynolds number of 16,000. In this case we see a considerably different situation in that while the local heat transfer coefficient is still periodic with period equal to one half the wavelength of the standing sound field, the axial location corresponding to velocity antinodes showed an increase in the local heat transfer rate. Correspondingly the axial locations representative of

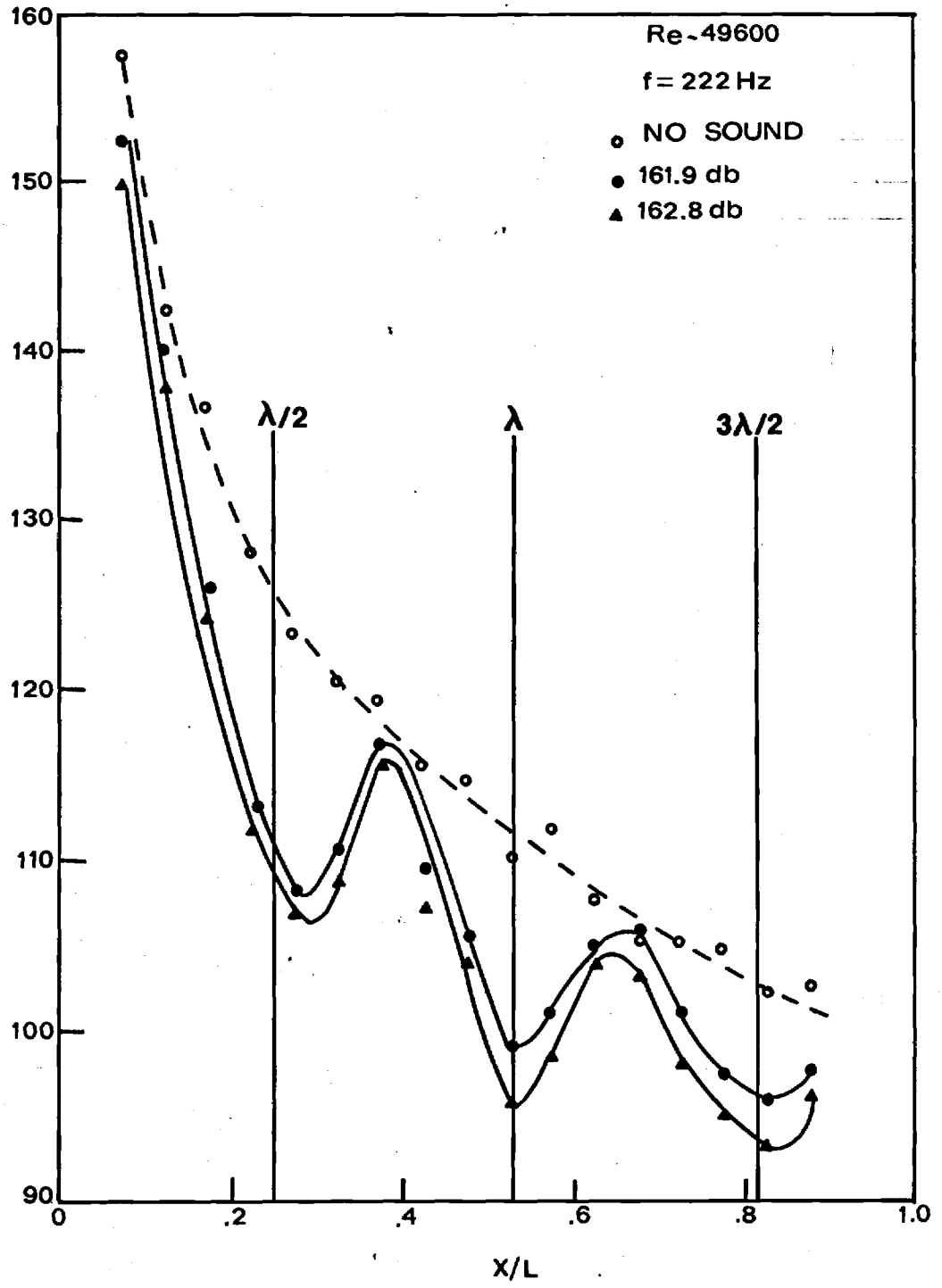

Figure 1. Local Nusselt Number Versus x/L for Various Sound Pressure Levels, Reynolds Number ≈ 49,600 (Reference 1).

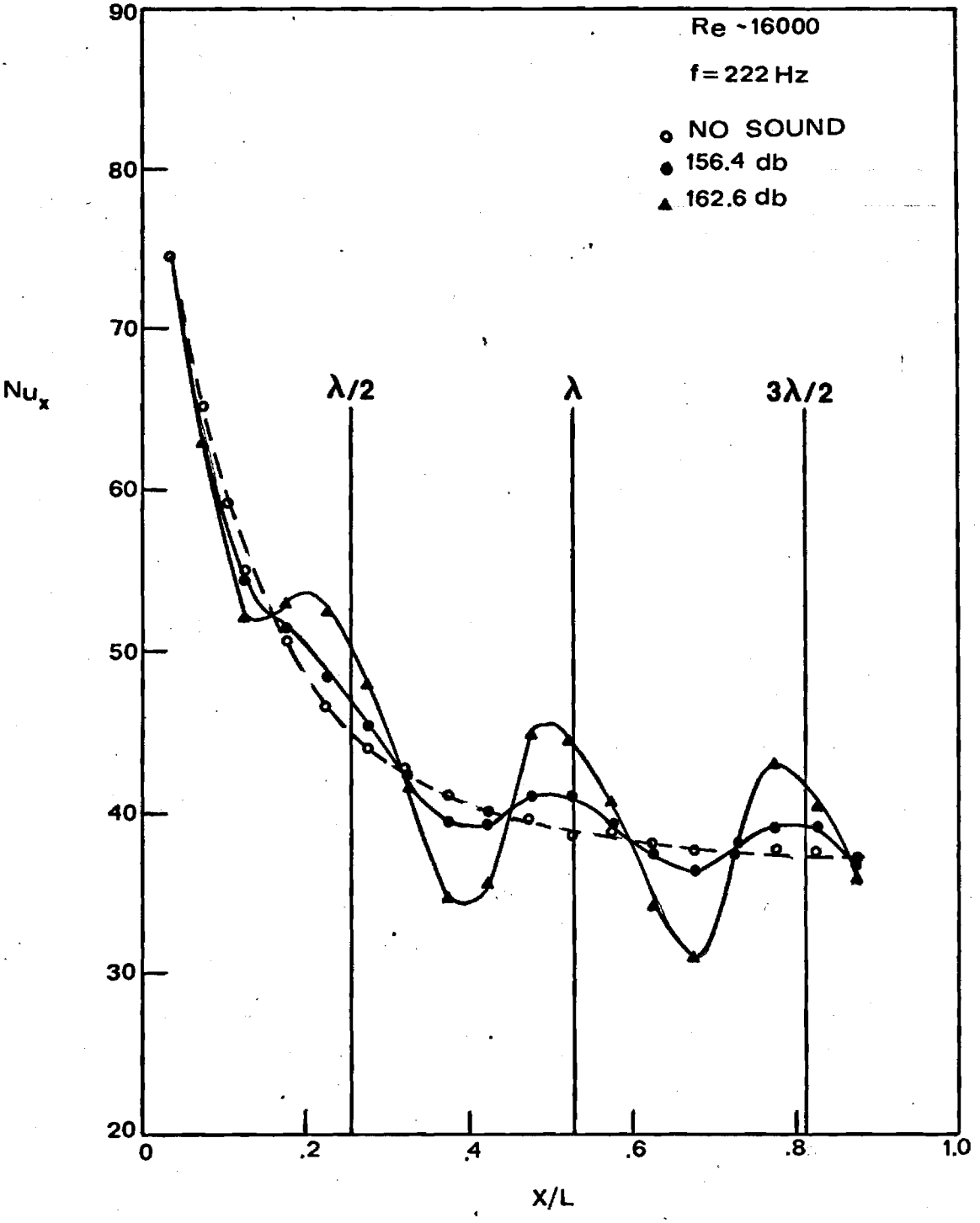

Figure 2. Local Nusselt Number Versus x/L for Various Sound Pressure Levels, Reynolds Number ≅ 16,000 (Reference 1).

velocity nodes showed a decrease in the local Nusselt number. The overall heat transfer coefficient obtained over the entire length of the test section is found to be virtually unaffected by the sound field for the low Reynolds number case, while for the Reynolds number of about 50,000 there was a net decrease due to the influence of the resonant acoustic field.

Intense resonant acoustic fields have been found to affect the transport of mass as well as the transport of heat. (Low and Hodgins[2]) Their results essentially were equivalent to the low Reynolds number data of Eastwood, et. al. in Reference 1. An increase of 170% was observed in the mass transfer rate at a velocity antinode for very low Reynolds numbers (150) and the enhancement of the mass transfer decreased as the Reynolds number increased. At or near velocity nodes the transport of mass was found to decrease with a threshold value in sound pressure level of about 130 db. In the heat transfer studies as well, the concept of a sound pressure level threshold (level below which no observable effects occurred) was noted.

The results of the low Reynolds number studies both in terms of heat transfer and mass transfer are well understood since they are identical to the results obtained when a laminar flow interacts with a longtudinally resonant acoustic field. In such a flow the acoustic field may be intense enough to generate time independent secondary flow patterns (acoustic streaming). As the through flow Reynolds number is increased, the strength of the acoustic field required to maintain these recirculating cells increases as well. If there is not sufficient acoustic energy to maintain the streaming pattern, the entire flow field changes character and so does the resulting heat transfer data as witnessed by the marked differences in Figures 1 and 2.

In attempting to determine the effects of periodic oscillations on normal flow processes, Michelson and Laurence[3] studied the interaction of a periodic fluctuation on flow in a duct. An important difference in this work when compared to the other studies mentioned here is that resonant conditions were not established in the test section. It was assumed that there was no correlation between the acoustic velocity component and the turbulent flow component and thus the total spectrum would be the addition of the individual spectra which implies a linear interaction phenomenon. Since the maximum sound pressure level considered was only 122 db it is not surprising that except for the frequency band containing the periodic fluctuation, they found no effect of the sound on the flow field.

The first attempt to study the interaction phenomenon in terms of longitudinal resonance conditions was due to Williams.[4] The results of that study showed that the resonant acoustic field, if intense enough, could cause a significant effect on the spectrum of all of the turbulence components when measurements were made near a velocity antinode (Figures 3 and 4). Measurements near a velocity node on the other hand, even for an extremely intense field, showed no effect (Figure 5). In addition it was found that the turbulent structure as characterized by the space microscale could also be significantly affected by the presence of the acoustic field. (Figure 6) From the results of the study (the spectrum of the three turbulence components with and without sound obtained using hot wire anemometer techniques formed most of the data) a physical flow model was proposed for an explanation of both the earlier heat transfer studies as well as for the spectrum data. The model was proposed only in light of the spectrum data obtained and did not have the benefit of any flow visualization to provide a clear understanding of the actual interaction mechanism.

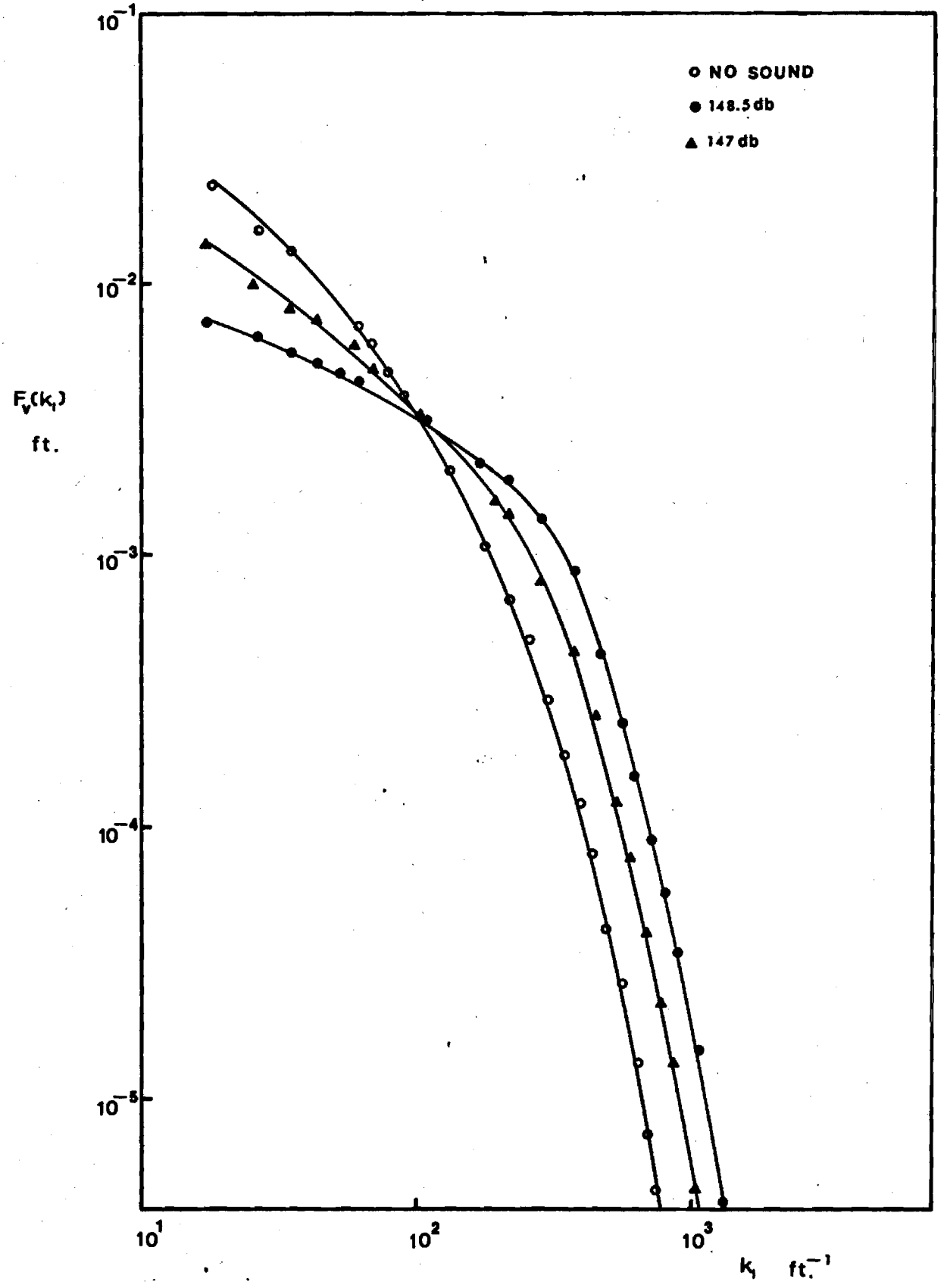

Figure 3. Normalized v' Spectra, Re = 50,000, $\frac{X}{D}$ = 25.5, $\frac{Y}{R}$ = 0.015.

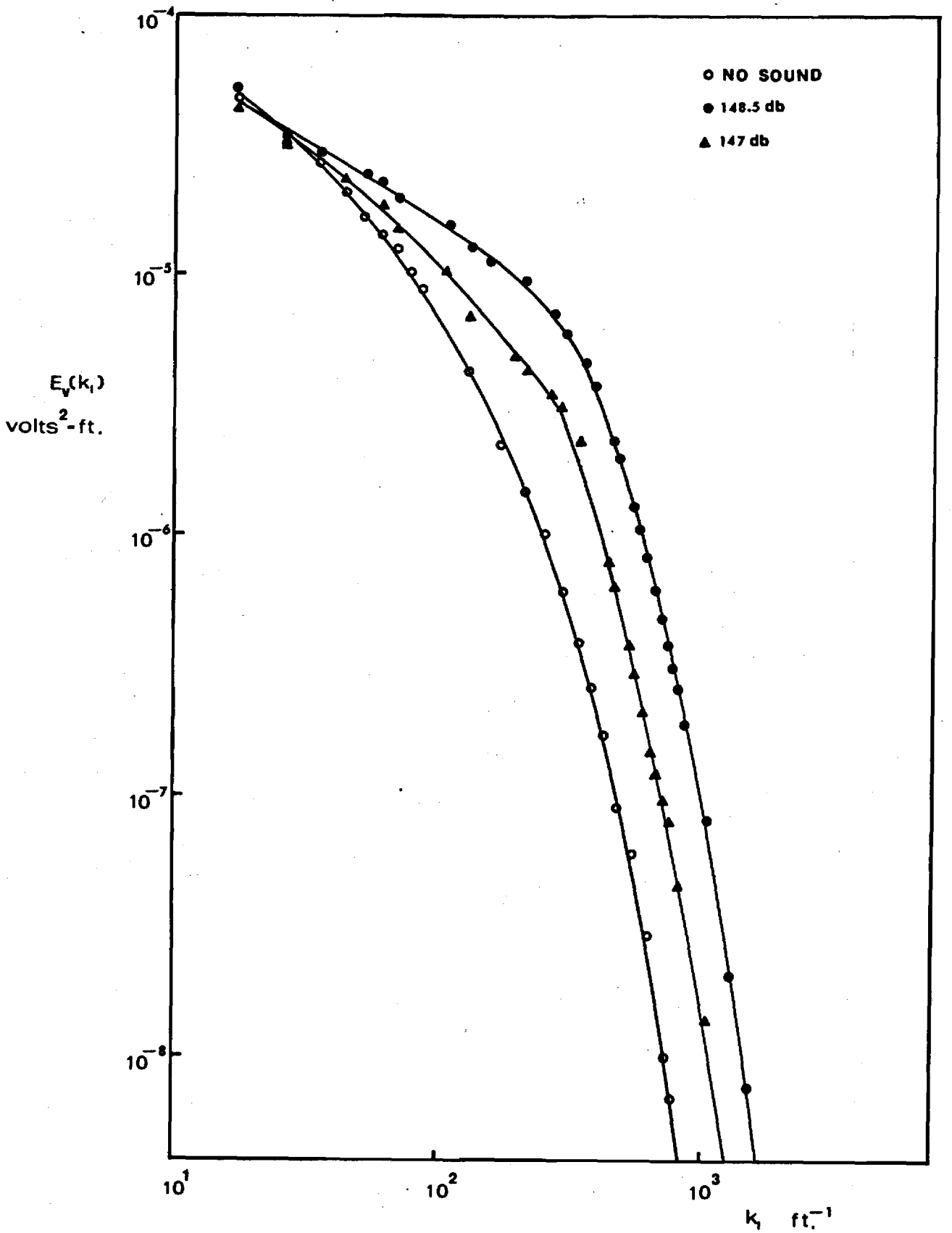

Figure 4. v' Spectra, Re = 50,000, $\frac{X}{D}$ = 25.5, $\frac{Y}{R}$ = 0.015.

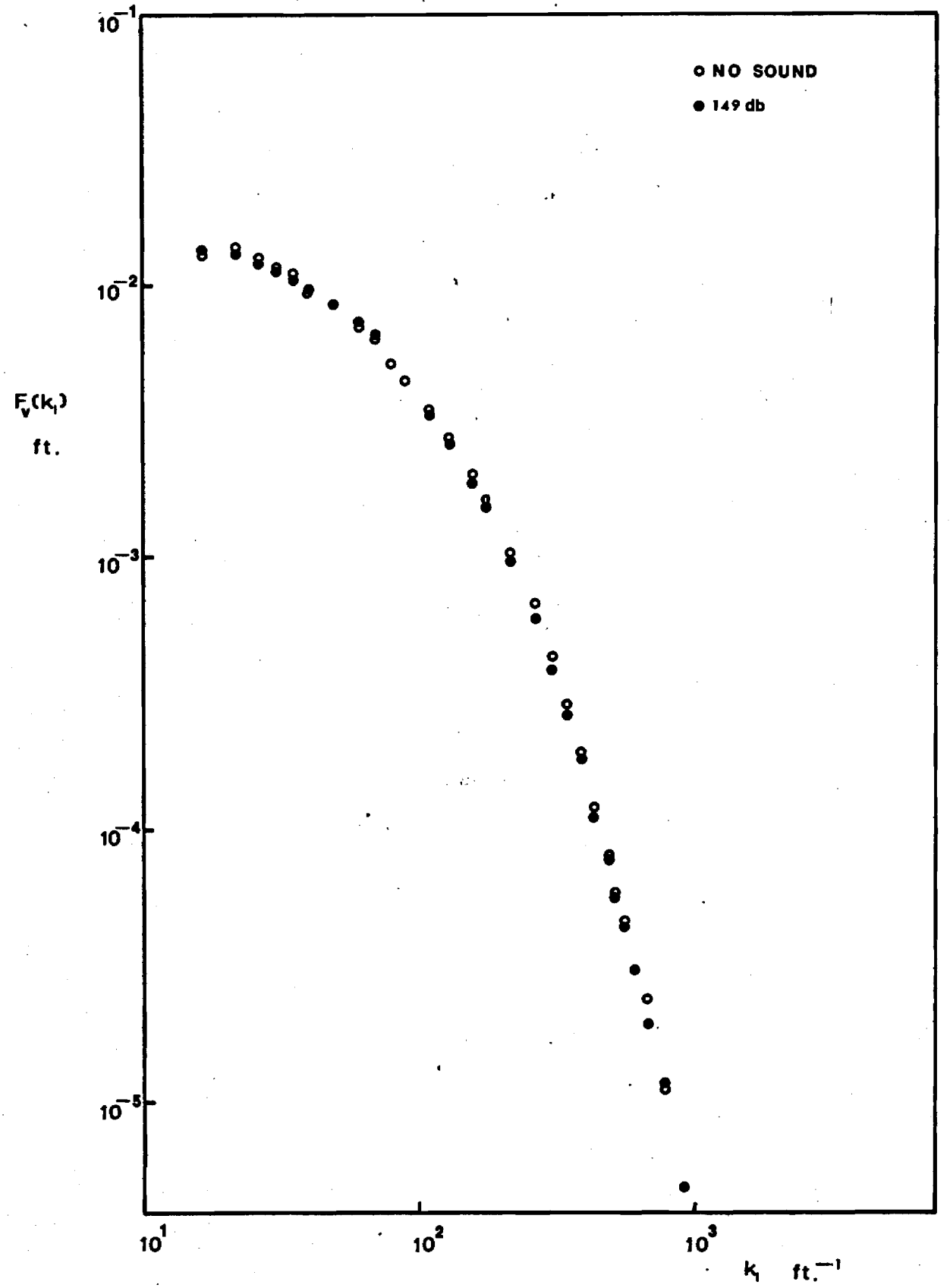

Figure 5. Normalized v' Spectra, Re = 50,000, $\frac{X}{D}$ = 19.5, $\frac{Y}{R}$ = 0.0125.

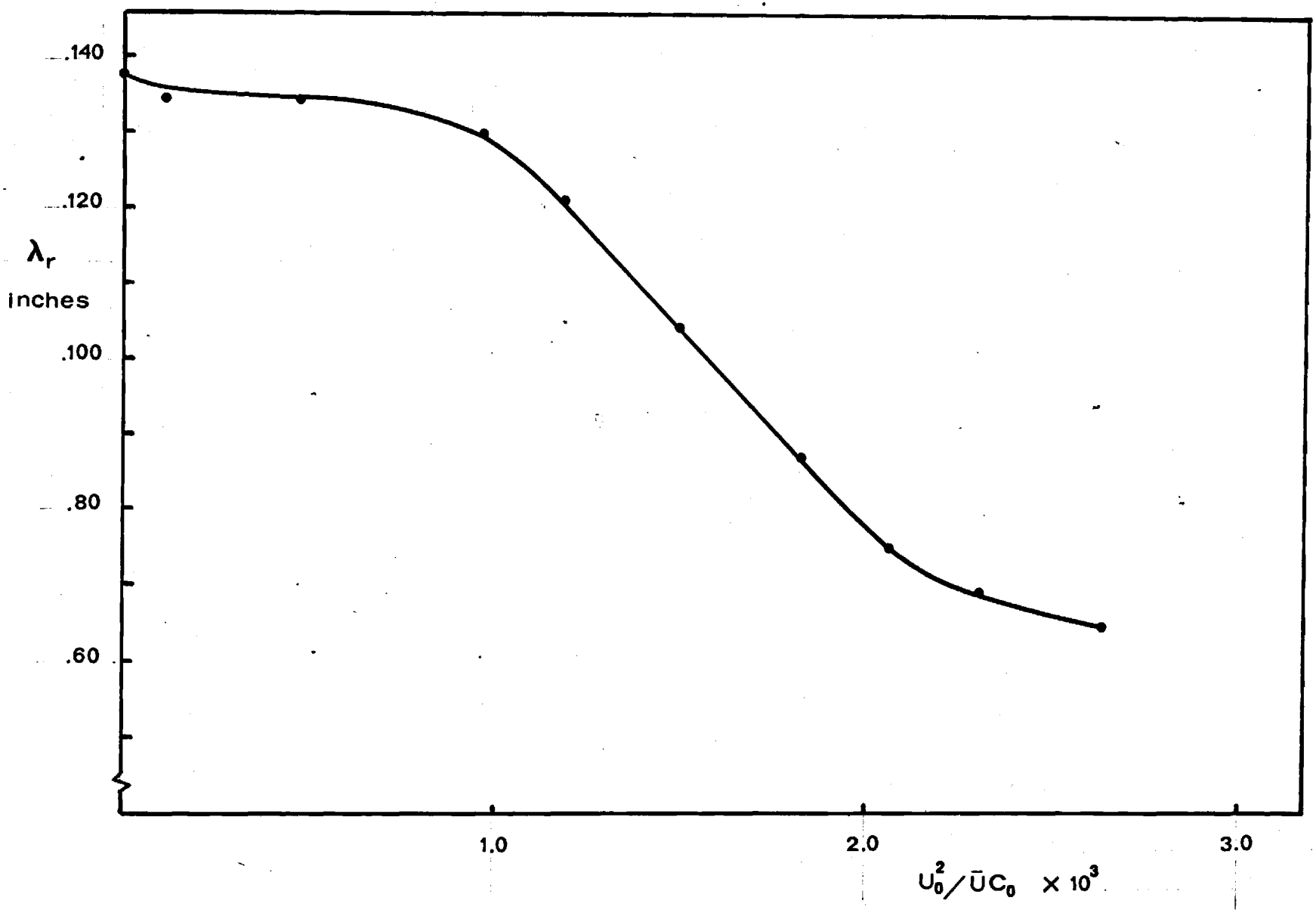

Figure 6. Microscale of the Turbulence from the Normalized v' Spectra, Re = 50,000, $\frac{X}{D} = 25.5$.

III. Objective

The objective of this study is to explore the interaction phenomenon in detail through additional hot wire anemometer spectrum measurements for the turbulence components, and in addition, to undertake a flow visualization study of the oscillating flow employing high speed photography. This data would then provide verification of the interaction models mentioned above or would provide a basis for a new model if the old ones are found to be physically in error.

IV. The Flow System

The flow system consists of two slightly different configurations depending on whether spectrum measurements or high speed photographs are being taken. The basic flow system will be discussed first and then the modifications required for flow visualization will be considered.

A schematic of the basic flow system is shown in Figure 7. Air enters a large 4 ft x 5 ft x 6 ft plenum chamber through a 1/2 horsepower blower, the inlet of which is monitored by a conical section that provides a variable inlet area. This provides the desired variation in flow rate necessary for the test cases considered. The air passes through a flexible coupling and straightening elements on its way into the plenum chamber. A series of furnace filters across the interior of the plenum, filter the air before it enters a large circular drum mounted flush with the upstream wall of the plenum. A bell mouth contraction is also mounted on the front wall of the plenum. The exit diameter of the contraction is 8 inches which allows the test section to fit concentrically and provides a boundary layer bleed. Thus the air entering the test section is the potential core

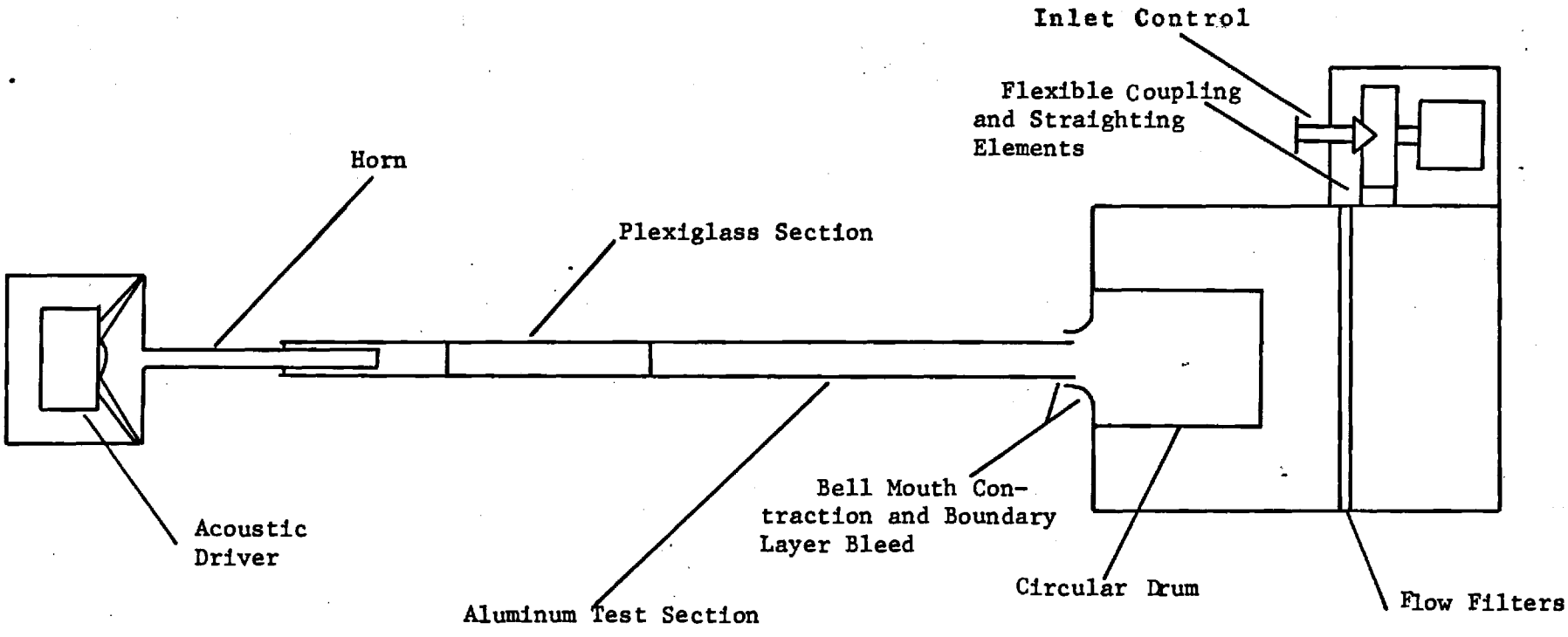

Figure 7. Schematic of Flow System.

of the contraction and the inlet profile is uniform. The test section itself is a twenty foot long aluminum pipe of inside diameter 6.06 inches and a wall thickness of 0.280 inches. A sharp edged inlet is provided to allow a minimum of inlet flow disturbance.

The first one foot of the test section is artifically roughned with gravel, whose diameters were typically from 0.06 inches to 0.18 inches, bonded to the wall with epoxy cement. This is to promote the growth of turbulence in the test section and is necessary for the low Reynolds number data in particular. Probe access holes of 0.375 inch diameter are provided every six inches for the first two feet of test section and every two feet thereafter. A probe access hole was drilled at a downstream velocity antinode as well (corresponding to the fourth harmonic of the fundamental pipe frequency) and it was at this location that the bulk of all the data was taken. At each probe access hole, and 90° to it, a static pressure tap was located. To prevent any leakage,particularly when the test section was in resonance, the probe access holes other than the one in use were sealed with plexiglass plugs, and the pressure taps were sealed as well.

The acoustic field was generated with the driver-horn assembly located at the test section exit. The horn was a piece of copper tubing with an outside diameter of 2.0 inches and a nominal length of 49 inches. The extent to which the horn extended into the test section depended on the frequency at which the test section was resonated. The horn was mounted concentrically in the test section by one fourth inch drill rods at an axial location one and one half inches from the exit. The acoustic driver was mounted in a stiffened plywood box whose dimensions were 21 inches x 25 1/2 inches x 25 1/2 inches. The entire assembly of horn and box was mounted on rails so

that the horn could be properly positioned axially in the test section.

The basic flow system was modified only slightly for the flow visualization. The aluminum test section was cut so that a clear plexiglass test section could be inserted in place of the aluminum piece. The length of the plexiglass section was six feet. One consequence of purchasing a standard piece of plexiglass tubing was that the dimensions were not perfectly compatable with the aluminum pipe. As previously mentioned the aluminum pipe had an inside diameter of 6.06 inches, and a wall thickness of 0.28 inches, which made the outside diameter 6.62. The plexiglass section had an inside diameter of 6.00 (as nearly as could be measured since it was not perfectly round), and a wall thickness of 0.250, and hence an outside diameter of 6.50 inches. In order that the inside surfaces formed a smooth junction, the plexiglass was first turned in a lathe and later hand sanded until it could be matched to the aluminum pipe at both ends. This involved a tapered interior surface at the joints and the 0.03 inch radial change was accommodated by an axial distance of about four inches. The exterior mismatch (outside diameters) was taken care of by shimming the plexiglass pipe at the mating collars where the joints were secured.

V. Instrumentation

The sound field was generated by an Altec-Lansing Model 515 B low frequency driver powered by a Hewlett Packard Model 206 A oscillator and an Altec Model 260 A amplifier. Since the driver had a continuous power rating of 35 watts, it was necessary to monitor the power being dissipated in the voice coil and this was done with a Fluke Model 102 VAW meter.

The spectrum measurements were made with Thermo-Systems Model 1051-1 hot-wire anemometers and a Model 1015-C correlator used as a sum-difference

unit for two wire measurements. The probes employed were of standard configuration for the determination of the longitudinal, radial, and circumferential components. They were a Model 1210-T 1.5 single wire probe, a Model 1240-T 1.5 X-array, and a Model 1241-T 1.5 X-array all manufactured by Thermo-Systems. They were positioned radially by an L C Smith Model BBS 8180 Probe Actuator and Model ABI-3 Indicating Control so that radial travel to 0.001 inches could be carefully monitored. The analysis of the hot-wire signals was performed on a Bruel and Kjaer Model 2107 frequency analyzer and a Hewlett Packard Model 302A frequency analyzer. The Brueland Kjaer frequency analyzer had a variable bandwidth equal to 6% of the center frequency. Bandwidth measurements showed this to be about equal to an effective bandwidth of 10%. In general this was found to be too wide, particularly for the interaction spectrum measurements so the Model 302A was used. The bandwidth for the Model 302A was not a function of the center frequency and was 7 Hz. This allowed good discrimination especially at high frequency. The meters on both instrumentations had only two separate time constants (the H-P meter had only one) and it was not possible to read the fluctuations in bridge voltage accurately. Therefore the Bruel and Kjaer Model 2417 random noise voltmeter was employed and a time constant as long as 100 seconds could be obtained. This was particularly valuable for low frequency data at low Reynolds numbers. The instrumentation was powered through a Sorenson Model 2501 AC voltage regulator, and during all data runs the hot-wire output signals were continously monitored by a Tektronic Model 502A dual beam oscilloscope. The sound field was monitored with a Bruel and Kjaer Model 4136 one quarter inch condenser microphone and associated cathode follower. The microphone cartridge was mounted flush with the upper surface of the test section and was located axially at a pressure antinode. The mounting assembly consisted of a brass bushing and a "O" ring seal to prevent any leakage of acoustic energy.

Calibration of the hot-wires was carried out using a Thermo-Systems Model 1125 calibrator and a Merriam Model 34FB2 micromanometer. The microphone was calibrated with a Bruel and Kjaer Model 4224 pistonphone.

The high speed photography was carried out through the use of a Red Lake Laboratories Hy-Cam 16 mm high speed camera. More information in regard to this phase of the study will be provided in a section on photographic technique and results.

VI. Smoke Generation and Injection System

A schematic of the system used to generate the smoke traces is shown in Figure 8. The smoke was generated by the burning of oil soaked cigars pressed into a 13 1/2 in long section of 3/4 inch steel pipe. The pipe was pressurized by a pressure regulated air supply. The generated smoke was bubbled through a flask containing water and the flask was inserted into an ice bath. By bubbling the smoke through the cold water, the moisture content in the smoke could be increased and the smoke was thus made much more visible when injected into the test section. The smoke left the flask after being filtered through a layer of steel wool and proceeded to a "T" junction in the injector system. The actual volume flow rate of the injected smoke could be controlled by either reducing the upstream pressure, opening the bleed value in the "T", or both. The injector itself which was mounted flush with the wall of the plexiglass test section was made out of stainless steel tubing with an outside diameter of 0.156 inches and a wall thickness of 0.015 inches. By using two or three oil soaked cigars in the pipe, a continuous flow of smoke could be generated for from ten to fifteen minutes which was more than enough time to make three or four data runs under varying acoustic and mean flow conditions.

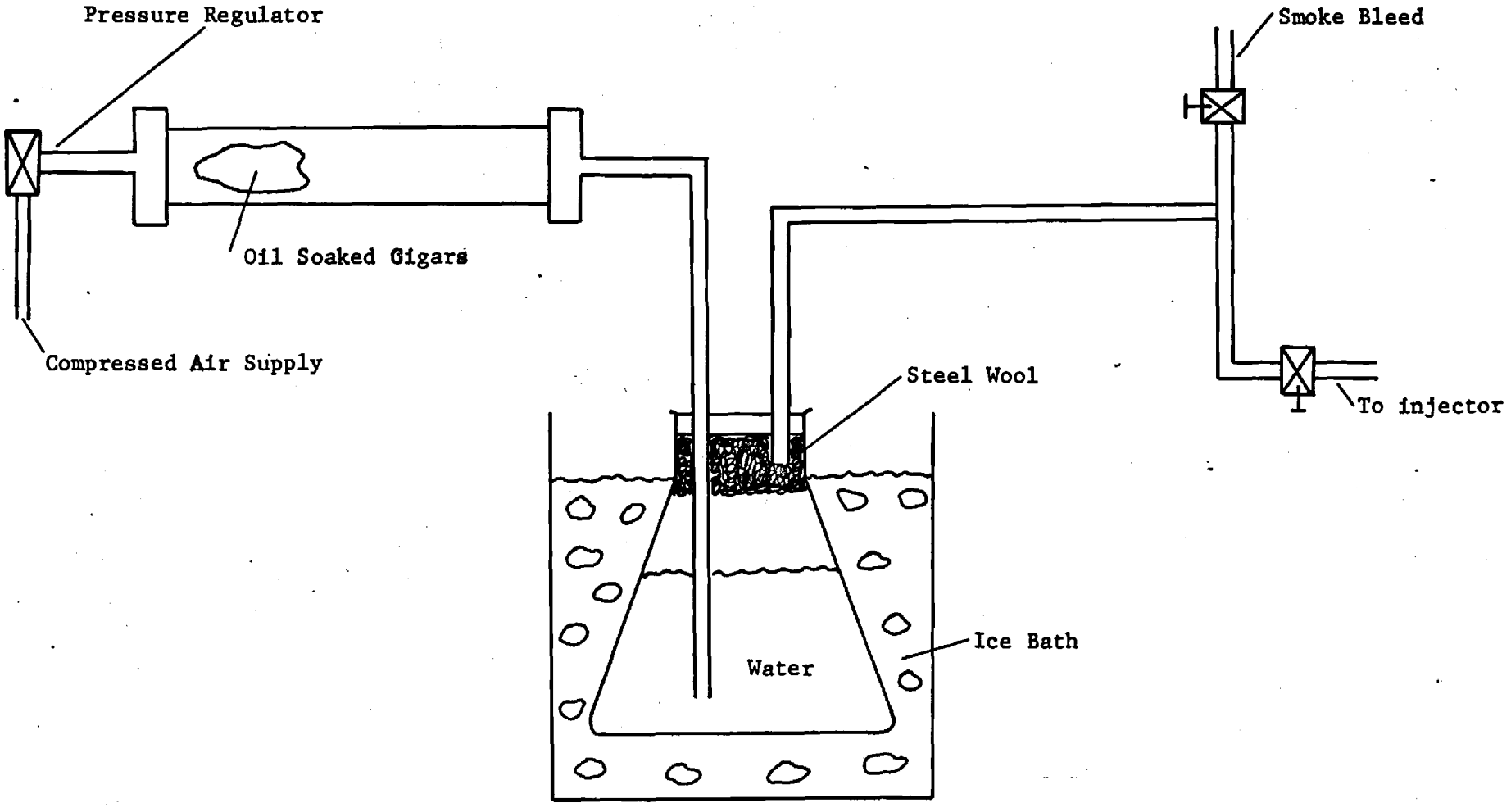

Figure 8. Schematic of Smoke Generation System.

VII. Longitudinal Acoustic Resonance in the Test Section

Acoustic motion is most generally thought of as a small perturbation on a mean or equilibrium condition. This equilibrium condition may be the steady flow of a fluid or a static fluid condition. The static fluid situation leads to a rather simple separation of the perturbation parameters from their mean flow counterparts and allows the solution of the governing equations. The separation of the mean quantities from the fluctuating quantities may be carried out in the presence of a steady mean flow as well but the resulting equations are more complex. Normally, linearizing approximations are made if the perturbation is small in comparison to its equilibrium counterpart, and this is generally acceptable for moderate acoustic intensities. In many analyses viscous effects are not considered so that the solution to the linear wave equation and other governing relations provides all the necessary information about the phenomenon. An important parameter which yields information about the extent of the viscous region near a solid boundary is the A.C. boundary layer thickness defined by

$$\delta ac = \sqrt{\frac{2\nu}{f}},$$

where ν is the kinematic viscosity of the fluid and f is the frequency of the periodic disturbance. Outside of this region the fluid is assumed to behave as though it were inviscid. To get a feel for the magnitude of this term, the A.C. boundary layer thickness for an oscillation of 110 Hz in air at a temperature of 75°F would be 0.00834 inches. While this is a very thin layer, it is in this region where viscous effects dominate over convective effects that secondary or time independent flows originate when strongly resonant acoustic fields interact with solid boundaries. The concept of

secondary flow cells was alluded to earlier in discussing the heat transfer results for laminar and low Reynolds number turbulent flows.

In the description of the resonant condition prevailing in this study the initial consideration will be presented assuming inviscid conditions and later a solution for the acoustic particle velocity will be given with viscous effects included. The inviscid solution assuming a single frequency disturbance with both leftward and rightward waves of equal intensity is given in (5). The solutions for acoustic pressure and acoustic particle velocity are

$$P'(x,t) = \rho C_o U_o \, \mathrm{Sin}\left(\frac{\omega x}{Co}\right) \mathrm{Sin}(\omega t)$$

$$u_1(x,t) = -U_o \, \mathrm{Cos}\left(\frac{\omega x}{Co}\right) \mathrm{Cos}\ (\omega t)$$

The wavelength λ of the wave is that value of x for which

$$\frac{\omega x}{C_o} = \frac{\omega \lambda}{C_o} = 2\pi$$

and thus

$$\lambda = \frac{2\pi C_o}{\omega} = \frac{C_o}{f}$$

From the form of the solution, which corresponds to organ pipe resonance, a standing wave pattern can be recognized, and velocity and pressure nodes are identified with particular zeros of $\mathrm{Cos}\left(\frac{\omega x}{C_o}\right)$ and $\mathrm{Sin}\left(\frac{\omega x}{C_o}\right)$. The axial locations for which $\mathrm{Cos}\left(\frac{\omega x}{C_o}\right)$ is identically zero correspond to velocity nodes which are seen to be pressure antinodes as well. The boundary conditions at the ends of an open-open pipe are (if no interaction with the surroundings is considered) that both ends are velocity antinodes. Since the distance between two adjacient velocity antinodes (or nodes) is one half wavelength, it is clear that the wavelength of the fundamental frequency is twice the geometric length of the

pipe. Thus

$$\lambda = 2L = \frac{C_o}{f_o} \quad \text{or} \quad f_o = \frac{C_o}{2L}$$

The harmonic frequencies for the pipe are then integral multiples of the fundamental f_o or

$$f_n = nf_o \quad n = 1,2,3...$$

While the locations of velocity and pressure nodes could be easily determined from the above results if the frequency was specified, it has been found experimentally that the velocity antinode does not occur exactly at the end of the duct. The antinode occurs slightly outside the duct and the correction as given by Wood (6) is

$$L_e \equiv L + 0.82\ D$$

Since the effective length is greater than the actual geometric length, the locations of the nodes and antinodes would be shifted (but only slightly) due to an increase in the wavelength. Using the corrected length, the locations of the nodes and antinodes were predicted by the theory for the frequencies of interest. In addition a saddle was built for the microphone so that it could be made to axially traverse the test section when it was in resonance. The distance between pressure minimums was easily obtained by measurement, and hence the locations of the pressure nodes as well as the actual half wavelength was determined experimentally. These experimental locations were compared with the locations found analytically and at the frequency employed in this study, the agreement was good. For example the first velocity antinode (with respect to the exit) is 1.1 inches nearer the exit than predicted and the second antinode in velocity is 0.50 inches farther from the exit then predicted, for a frequency of 110 Hz. The deviation of

of 1.10 inches and 0.50 inches are with respect to actual distances of about 59 inches and 121 inches so that the percentage variation is small. The measured half wavelength was 62.3 inches as compared to a theoretical value of 61.5 inches (both based on a frequency of 110 Hz and a corrected test section length).

Since we have considered the solution to the wave equation for acoustic pressure and particle velocity, and since the acoustic pressure manifests itself in the microphone output as the sound pressure level (SPL), some relationship between these parameters should be described. The sound pressure level is defined as

$$SPL = 20 \log_{10} \frac{P'_{rms}}{Pref_{rms}}$$

where $Pref_{rms}$ = 0.0002 μ bar. The peak value of the sound amplitude is related to the rms value through the form of P'(x,t) which for a resonant field from a harmonic oscillation is easy to determine. From the definition of SPL and the plane wave solution obtained for the resonant condition, it is possible to solve for the maximum particle velocity of the acoustic field. The solution is

$$U_o = 0.20\, C_o\, C_p\, 10^{\left(\frac{SPL-180}{20}\right)}$$

where C_p = ratio of standard atmospheric pressure to the local static pressure in the test section. There is a temperature dependence as the isentropic speed of sound depends on the square root of the absolute temperature. From the form of the solution it is clear that the variations of U_o with sound pressure level is very dramatic, particularly at high levels of intensity.

It was felt by the author in Reference 4 that a key to the interaction effect was a comparison of the local mean velocity of the flow to the acoustic particle velocity. This was inherently linked to the question of whether flow reversal was likely to occur or not. In order to answer a question such as this, a solution for the acoustic particle velocity (along the tube axis) should be determined when viscous effects are included. A solution to this problem was obtained, (5), and is given below. This is an approximate solution which is valid for large values of r'

$$u_1(r',x',t) = U_o \cos(\pi x') \left[\cos(2\pi t') - \frac{1}{\gamma} \exp(-R'(1-\gamma) \cdot \cos(R'(1-\gamma) - 2\pi t')\right]$$

where $\pi x' = \frac{2\pi x}{\lambda}$ = dimensionless axial distance

$$R' = \frac{R}{\delta ac}; \quad r' = \frac{r}{\delta ac}; \quad \gamma = \frac{r}{R}; \quad \delta ac = \sqrt{\frac{2\nu}{f}}$$

and $t' = \frac{\omega t}{2\pi}$ = dimensionless time

From this result it is seen that the magnitude of the axial velocity component for a given time, axial and radial location is directly related to the maximum acoustic particle velocity U_o, found previously. Figure 9 shows the dependence of u_1 on both radial location and sound pressure level for a fixed axial location (here a velocity antinode). Comparison of profiles such as these with the actual turbulent velocity profile is helpful in predicting the occurance of back flow or flow reversal in the test section.

VIII. Spectrum Analysis and its Utility in Turbulent Flow Fields

In many turbulent flow fields, but this one in particular, it is impossible to gain enough information about the character of the flow by employing mean square measurements. If it is important to obtain detailed information about small scale structure or energy transport, it is

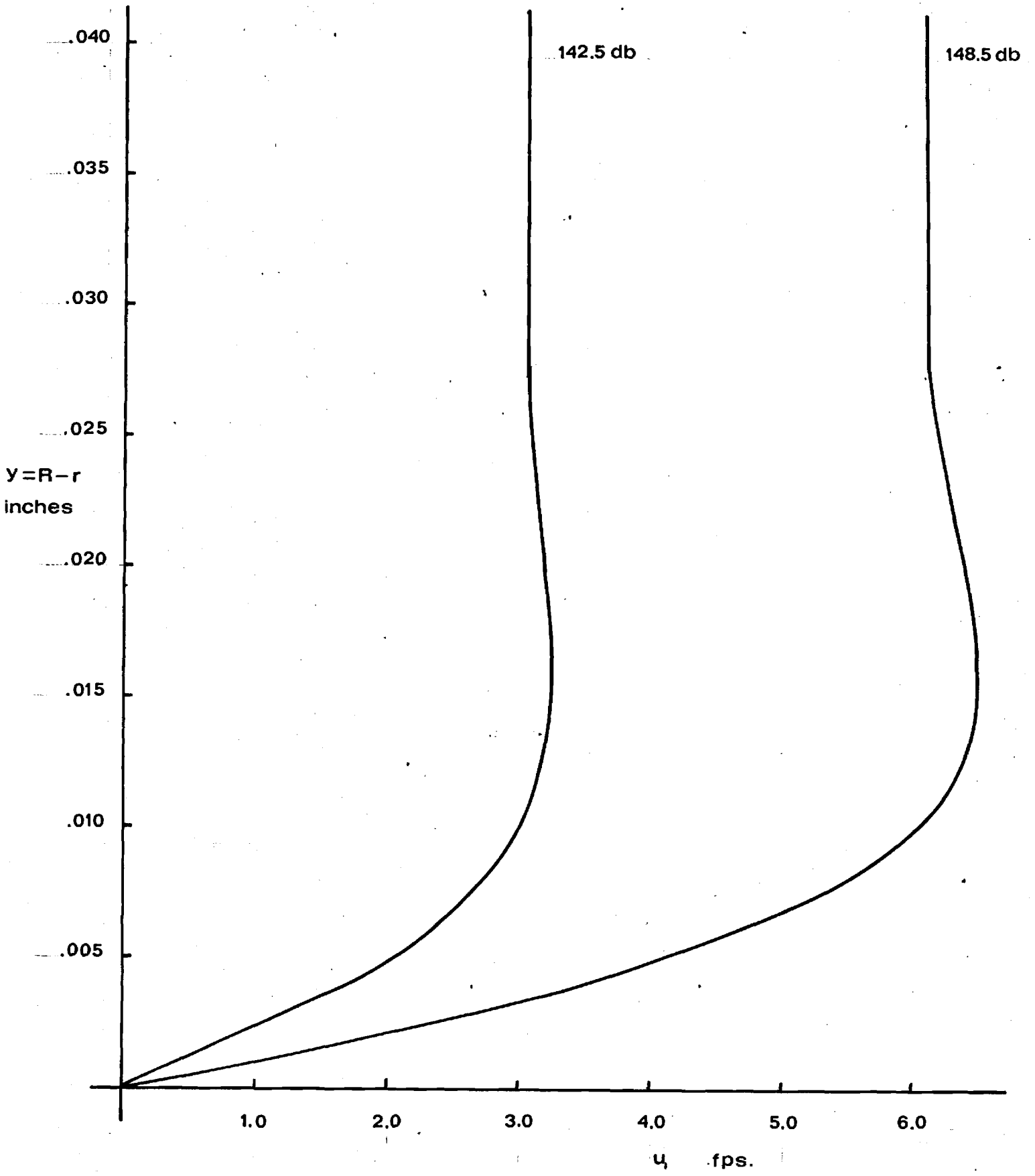

Figure 9. Axial Acoustic Particle Velocity.

necessary to resort to measurements of the harmonic content of the velocity components. Due to the complexity of most turbulent flow fields experimental techniques are required since the theory related to spectrum analysis has been developed for flows that are homogeneous or isotropic. In the case considered here the flow field is not homogeneous, isotropic, or even fully developed.

The spectrum measured by the hot-wire anemometer is the Taylor one-dimensional spectrum or time spectrum. What this physically represents is a spatial distribution of energy along a surface K_1 = constant where K_1 is the wave number defined by $K_1 = \frac{2\pi f}{\bar{U}}$. The basis for the use of the one dimensional spectrum and its intrepretation comes from the consideration of the earlier work of Taylor (7). Quoting from Taylor's paper

> "If u, the component at a fixed point of turbulent motion in the direction of the main stream at a point in a wind tunnel, is resolved into harmonic components, the mean value of $\bar{u}^2$ may be regarded as being the sum of contributions from all frequencies. If $\bar{u}^2 F(f)$ is the contribution from frequencies between f and f + df then
>
> $$\int_0^\infty F(f)df = 1.0"$$

A mathematical proof that $\bar{u}^2$ was actually the sum of contributions from all frequencies had been given earlier by Rayleigh.

It is well known by considering the operation of a hot wire anemometer that the voltage fluctuations from the wire are proportional to the fluctuations in turbulence velocities. The proportionality constant or constants may be determined by an accurate calibration of the wire or wires. With this fact in mind, the harmonic analysis of the turbulent velocity fluctuation is

reduced to the harmonic analysis of the voltage fluctuation caused by the turbulence. This type analysis may be carried out using narrow band electronic filters. The energy spectral density E(f) may be defined as follows:

$$E(f) = \lim_{B \to 0} \frac{\bar{e}_f^2}{BH^2}$$

where B is the filter bandwidth, H is the gain of the filter at the center frequency, and $\bar{e}_f^2$ represents the mean squared filter output at the center frequency f. Regardless of the type filter used it has a non zero bandwidth but the actual frequency distribution of the turbulence is broad (extends over several octaves) and thus a smoothing of the distribution is obtained. Thus the error is approximating the energy density to be

$$E(f) = \frac{\bar{e}_f^2}{BH^2}$$

is small. Two types of filters are commonly used; one utilizing a constant fixed bandwidth, and the other employing a constant percentage bandwidth. For the latter filter the bandwidth increases with frequency and is a constant percentage of the center frequency. Both types were available for this study and were previously mentioned in the section on instrumentation. The Bruel and Kjaer Model 2107 frequency analyzer had a tunable filter with a minimum bandwidth (down 3db) of 6%. This actually turned out to be an effective bandwidth of about 10% as obtained from a graph of gain squared as a function of frequency. A bandwidth as wide as 10% of the center frequency was too wide to allow discriminatory look at the spectrum that was required and thus it was necessary to use the Hewlett-Packard Model 302A frequency analyzer. This analyzer has a three db bandwidth of 7Hz for all

frequencies and although this makes it somewhat wider than the Band K Model 2107 at very low frequency, it was superior at high frequency. The reason that an extremely narrow filter is necessary is that frequencies very close to the resonant frequency of the sound field (and its harmonics) can be analyzed without being weighted by the pure tone components associated with the sound field. (It should be noted at this point that the sound field itself is free of harmonies, but since the hot wire anemometer is a nonlinear device, harmonics and possibly subharmonics may appear on the wire output.)

With the filter characteristics known, the energy spectral density may be computed as a function of frequency once the energy contained in the band centered at f_c is obtained by measurement. Another useful function that is available once the energy spectral density has been found is the normalized energy density defined as

$$F(f) = \frac{E(f)}{\bar{e}^2}$$

and from earlier results due to Taylor it is clear that

$$\bar{e}^2 = \int_0^\infty E(f)df.$$

Since the hot wire voltage fluctuation is proportional to the velocity fluctuation through the sensitivity, then

$$F(f) \alpha \frac{\bar{u}^2_f}{\bar{u}^2}$$

where $\bar{u}^2_f$ represents the velocity fluctuations in the bandwidth centered about the frequency f_c and $\bar{u}^2$ represents the total mean square velocity fluctuations over all frequencies.

The use of the one-dimensional wave number defined previously allows the comparison of energy spectra in regions of different mean velocity $\bar{U}$ and allows a convenient representation of spectrum data. Due to the relationship between K_1 and f it is possible to write that

$$F(K_1) = \frac{\bar{U}}{2\pi} F(f)$$

where $F(K_1)$ is also a normalized function such that

$$\int_0^\infty F(K_1) dK_1 = 1.0$$

Taylor's work also showed the relationship between the turbulent energy spectra and the auto correlation in that they are Fourier transforms of one another. Thus it is sufficient to measure only one or the other. (Inherent in the above consideration is Taylor's hypothesis of the "frozen turbulence pattern" in which the longitudinal correlation coefficient $R(x)$ is equal to the auto correlation $R(\tau)$.) Correlation measurements yield valuable information about the turbulent structure and hence eddy size, so spectrum measurements should yield the same type of information. The microscale λ_x is thought of as being representative of a measure of the smallest eddies in the flow, that is those eddies where the dissipation of turbulent energy into thermal energy is taking place. The microscale has been defined from the form of the correlation function $R(x)$ near the origin. (Qualitatively we would expect correlation curves which fall away slowly with increasing separation distance x are representative of an eddy structure made up predominantly of large eddies. The converse would be true for small eddies.) A dissipation scale for the lateral correlation coefficient would be defined in a similar manner. The actual expressions for both the longitudinal micro- and macroscales defined in terms of the longitudinal correlation function

R(x) are

$$\frac{1}{\lambda_x^2} = \frac{1 - R(x)}{x^2} \quad \text{and} \quad \Lambda_x = \int_0^\infty R(x)dx$$

The macroscale, or integral scale, is thought of as an average size of the eddies in the flow. Due to the Fourier transform relationship between the spectrum function and the correlation function the above results may also be written as

$$\frac{1}{\lambda_x^2} = \frac{1}{2} \int_0^\infty K_1^2 \, F_u(K_1)dK_1 = \frac{2\pi}{U} \int_0^\infty f^2 \, F_u(f)df$$

and

$$\Lambda_x = \frac{\pi}{2} \lim_{K_1 \to 0} F_u(K_1) = \frac{U}{4} \lim_{f \to 0} F_u(f)$$

The importance of the harmonic analysis has been mentioned for a normal turbulent flow, but an analysis of this type is of even greater value in a flow that involves pure tone components such as the reasonant acoustic condition encountered here. With the large periodic velocity component superimposed on the normal velocity fluctuation, the mean square voltage output from the hot-wire anemometer would be heavily weighted at a single frequency or its harmonics. The result would be that the voltage output would have lost its "turbulent character" due to the lack of randomness and would simply be a periodic phenomenon with small scale random fluctuations. However, a frequency analysis of this signal, employing a narrow band filter, would allow bands close to the resonant frequency or its harmonics to be investigated critically and thus an analysis of the random turbulence could be made in the presence of the periodic disturbance. Thus any significant change in the overall energy in a given band, removed from the resonant frequency, would be an indication of the effect of the acoustic field on the normal turbulence.

A considerable amount of the data in this report is presented in the form of the normalized energy density as a function of the wave number K_1. In order

to obtain the normalized energy density, it was necessary to integrate the voltage contributions from all bandwidths, ie:

$$\bar{e}^2 = \int_0^\infty E(f)df$$

The actual lower limit on the integral was the 20Hz center frequency on the wave analyzer and the upper limit depended primarily on the electronic noise in the hot-wire anemometers and correlator. This upper limit varied from 1750 Hz to 2500 Hz depending on the flow Reynolds number and radial location.

It should be apparent that $\bar{e}^2_f$ in the bandwidths centered at the resonant frequency of the acoustic field and its harmonics was significantly larger than the normal turbulence level. Because of this any large scale fluctuations which could be attributed directly to the acoustic field were not included in the computation of the mean-square voltage $\bar{e}^2$ used for the normalization of the energy spectral density. The 7 Hz filter was narrow enough so that all of the general characteristics of the turbulence were retained even though it was necessary to omit certain discrete frequencies from the overall spectrum. It was felt that this was necessary to prevent the normalized energy density from being biased by an effect that was periodic rather than random.

While data displayed in terms of the normalized energy density $F(K_1)$ vs. K_1 have advantages, they also suffer the disadvantage in that the normalization process causes the absolute location of the spectrum curve to be lost. The fact that two different spectrum curves have the same value of $F(K_1)$ for a given wave number does not mean that they have the same energy at the wave number. It simply means that they have the same percent energy based on the

integrated mean-square voltage. It is important to keep this in mind when interpreting normalized energy density data. In order to establish the absolute location of the spectrum curves it is necessary to display the energy density on an $E(K_1)$ vs K_1 or an E(f) vs f basis. For a given frequency or wave number this function yields the actual energy associated with a particular center frequency. In order to determine whether a significant effect at a particular frequency can be attributed to the acoustic field it is advisable to consider both functions. The first, $F(K_1)$, provides information as to how the normalized energy is distributed among the wave numbers and also directly yields information about the micro- and macroscales of the turbulence. The second, $E(K_1)$, resolves the question of the actual energy in a given bandwidth and answers the question regarding the absolute location of the spectrum curve for a given electronic filter and flow condition. The data was analyzed and interpreted in light of these considerations.

IX. Photographic System and Technique

The 16 mm high speed motion pictures were taken with a Red Lakes Laboratory 16 mm Hy Cam camera employing Kodak 4-X Reversal Film No. 7277. The capabilities of the camera were such that speeds of 14000 frames per second could be obtained. All of the data in the report came from data runs with film speeds of 1000 to 3000 frames per second. Since the acoustic phenomena was periodic at a frequency of just over 100 cycles per second, the above mentioned film speeds allowed from 10 to 30 frames to display a cycle of oscillation. The camera was mounted on a tripod and the region of the wall of the test section where the smoke injection took place was centered in the field of view. In order to illuminate the smoke adequately for photographing

while reducing reflections off of the plexiglass test section, a method was devised to illuminate the field through a slit along the bottom of the test section. A shroud was built around the plexiglass and was spray painted a flat black. The slit formed by parts of the shroud was about one inch in width by 10 inches long. The light source was a 650 watt spot/flood light mounted below the test section and directed upward. Preliminary photographs were taken to establish the proper lens settings, film speed, and smoke injection rate so that maximum clarity and contrast could be achieved.

X. General Comments in Regard to Hot-Wire Anemometer Measurements

There are a number of pertinent variables that could be investigated in a study such as this. Some have constraints placed on them by certain capabilities of the facilities employed and other of the variables eliminate themselves from consideration simply because no significant effect is found in terms of the interaction of the resonant sound field and the normal turbulent flow. As was reported previously, the acoustic driver had a maximum continuous power rating of 35 watts. The result of this constraint, plus a safety factor in regard to the continuous operation of the driver, was that a sound pressure level of a maximum of 148.5 db. re. 0.0002 bar was obtainable at low Reynolds number. With the plexiglass test section in place the coupling was such that again a continuous sound pressure level of 148.5 db could be maintained. These numbers form the upper limits in regard to the level of the acoustic input in this report.

Other important variables in addition to the level of the acoustic input (SPL), were Reynolds number, axial location in test section (position in the acoustic resonance pattern), and radial location in the test section. These four variables can all be considered in regard to the investigation of each of the turb-

ulence components. As an example of these variables eliminating themselves so that all combinations need not be considered, it was found that with the levels of acoustic input attainable here, Reynolds numbers of above 40,000 were found to be unaffected by sound pressure levels up to 148.5 db. This was true in spite of the fact that measurements were made at a velocity antinode. This tied into the flow visualization data in that the smoke was injected and photographed only at a velocity antinode.

The data to be presented then is representative of measurements made at a Reynolds number of 40,000, an axial location corresponding to a velocity antinode (at the fourth harmonic), and the parameters varied are the radial location and the level of acoustic input. This is done for the longitudinal, radial, and circumferential components of the turbulence.

XI. Comments on Preliminary Measurements.

Preliminary measurements were made to determine the effect of Reynolds number, axial location, radial location and acoustic power input, while also assessing the use of two different wave analyzers in the spectrum analysis.

Initial measurements demonstrated that it was possible to maintain a continuous sound pressure level of 148.5 db re. .0002 μ bar with a sufficient safety factor for all Reynolds numbers considered. This maximum level was found to have little or no effect on the flow field for a Reynolds number of 60,000 and hence the Reynolds number was reduced to 40,000 for the data presented here.

Preliminary measurements were made at axial locations corresponding to $\frac{X}{D} = 28.0$ (the location of the nearest velocity antinode was $\frac{X}{D} = 30.3$) and while the Re = 40,000 flows were affected at this location, an access hole for the hot wire probe was drilled exactly at the velocity antinode to obtain

the maximum effect. This was also done so that the parameters of the hot wire study were identical if possible to those of the flow visualization study.

Radial location was also a consideration and preliminary measurements showed decreasing effects as the radial distance from the wall was increased. Due to the probe configurations it was possible to measure much closer to the wall with the single wire probe. So that all of the data for a single point in space could be presented (longitudinal, radial and circumferential velocity components) the minimum radial position corresponded to the minimum distance from the wall to the center of the X-array used for the radial component. Data is given for two separate values of radial location.

Two different wave analyzers were considered in the preliminary measurements (see section on instrumentation, Section V). After considerable data was taken and analyzed it was clear that the bandwidth of the Brueland Kjaer Model 2107 Frequency Analyzer was too wide to adequetly demonstrate the interaction effect, and hence all subsequent data was analyzed with the constant bandwidth Hewlett-Packard Model 302 A Wave Analyzer.

Preliminary flow visualization measurements were made to determine the proper lighting, camera f stop, film speed, and smoke injection rate. These measurements included photographs of the smoke in the normal turbulent boundary layer with no sound, photographs of the test section in longitudinal resonance with smoke being injected with no mean through flow, and finally the photographs of the interaction phenomenon itself. The parameters finally decided upon after these preliminary measurements were; slit lighting from the bottom of the test section with a single light of 650 watts, camera speed of 2000 frames per second, and an f stop setting of f 2.5.

XII. Final Results

Hot-Wire Anemometer Spectrum Measurements

Longitudinal Component

The data presented in Figures 10 and 11 depict both the normalized energy density and the energy density as a function of various levels of acoustic input for a fixed Reynolds number of 40,000. The radial position is 0.04 inches from the wall and the axial location of $\frac{X}{D}$ = 30.3 corresponds to a velocity antinode for the frequency of oscillation which is 110 Hz. The effect of the acoustic oscillations is manifested in a considerable increase in the energy over most of the frequency range, but the effect is most pronounced at the higher frequencies. At these frequencies and for a sound pressure level of 148.5 db, both the energy density and normalized energy density functions have been increased by more than one order of magnitude. In this situation, as indeed in all data to be presented, the harmonics of the sound field have not been presented in the spectrum. This increase in the energy content of the high frequency bands then must be due to a transfer of energy through the entire spectrum of frequencies since the acoustic oscillation was a pure tone at 110 Hz. As the level of the acoustic input is decreased to more moderate intensities the effect of the perturbation on the flow decreases as one would expect. For this component, (although it does not appear on the figure) data was also taken at 140 db and the effect was only very slight. While a threshold value per se was not sought, it would appear that it is only for sound pressure levels above 140 db that significant effects are to be found.

Figures 12 and 13 represent data for conditions similar to that previously considered in Figures 10 and 11 except that the radial position has been changed from 0.04 inches to 0.05 inches from the wall of the test section.

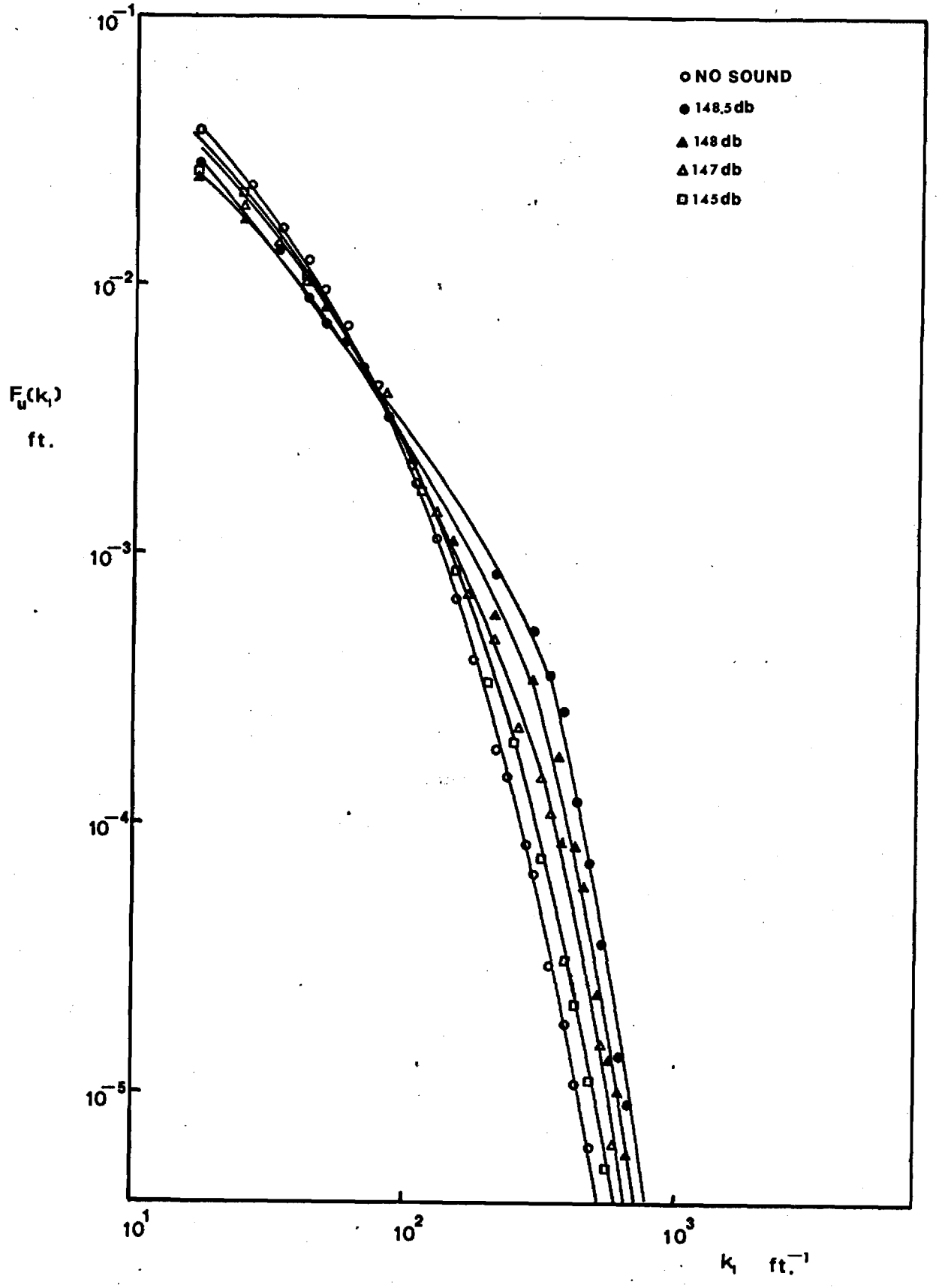

Figure 10. Normalized u' Spectra, Re = 40,000, $\frac{Y}{R}$ = 0.0132, $\frac{X}{D}$ = 30.3.

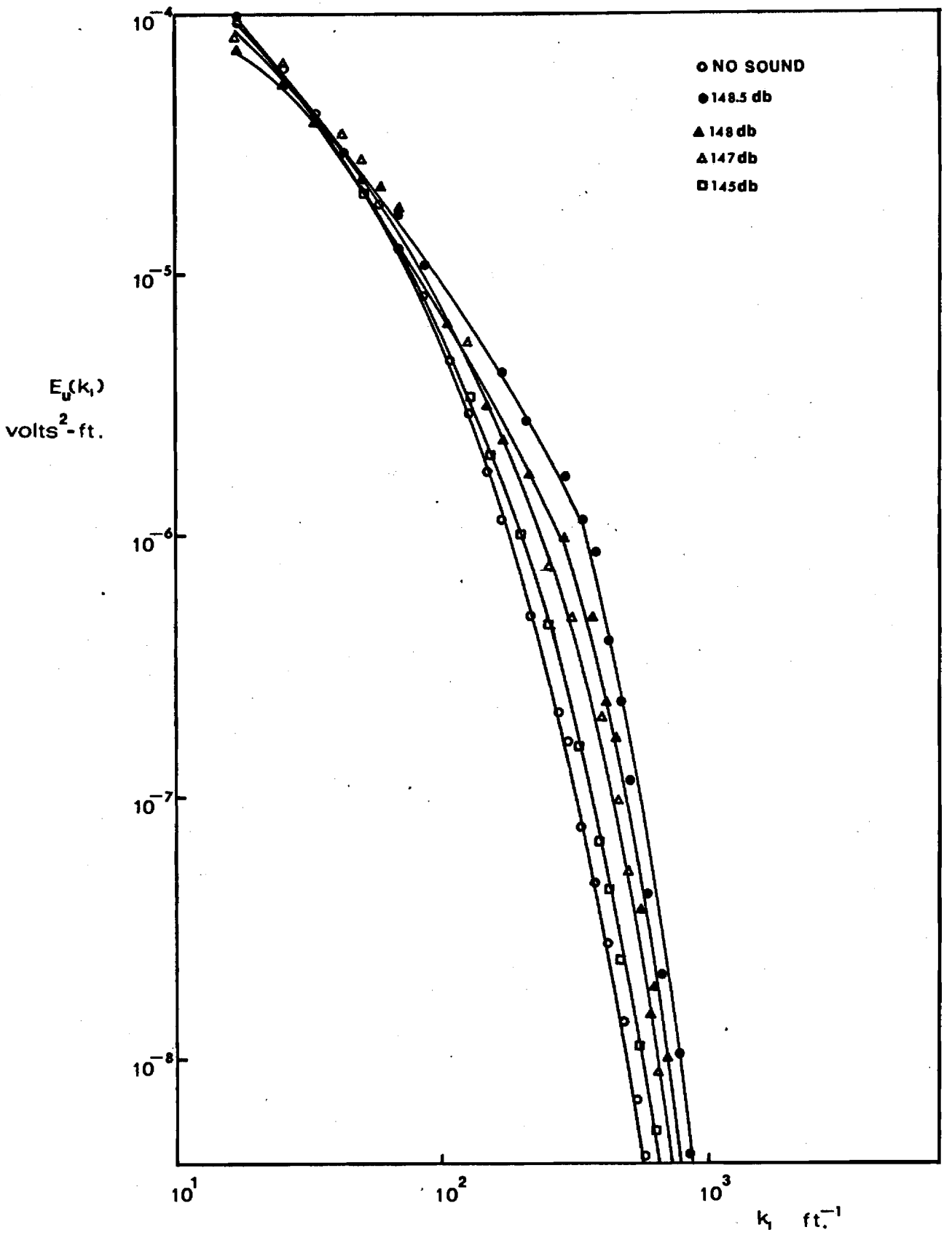

Figure 11. u'Spectra, Re = 40,000, $\frac{Y}{R}$ = 0.0132, $\frac{X}{D}$ = 30.3.

All other parameters are the same. The distributions again show the increase in the energy content of the high frequency regions of the spectra, but it may be noted that the actual interaction effect for the intensities shown is not as great as that in Figures 10 and 11. Thus the influence of the radial location as a parameter is seen in that for greater distances from the wall the effect of the acoustic field diminishes as one would expect.

For each radial location the spectrum of the longitudinal component was obtained for the following sound pressure levels; 148.5 db, 148.0 db, 147.0 db, 145.0 db, and 140.0 db. A no sound run was also made. In section VII the relationship between the normalized energy density function and the microscale of the turbulence was presented. From this relationship, and by numerical integration of the individual spectra, it was possible to obtain the microscale under varying conditions of acoustic input.

A question arises as to what other variable, pertinant to both the turbulent flow and the sound field, might be related to the interaction effect as demonstrated by the variation in microscale. It was shown in Reference 8 that the deviation from the no sound heat transfer data caused by the acoustic field could be correlated in terms of the following dimensionless parameter, $U_o^2/\bar{U}C_o$. As previously seen U_o the maximum amplitude of the acoustic particle velocity depends strongly on the sound pressure level. Based on these considerations the longitudinal microscale λ_x has been plotted as a function of this parameter in Figures 14 and 15. The change in the microscale is seen to be that of a decrease over the corresponding no sound value, and in both situations $y = 0.40$ and $y = 0.50$ the minimum value of λ_x occurs for the maximum sound pressure level (SPL) of 148.5 db. The small effect of the sound field on the spectra at a SPL of below 147.0 db as shown in Figures 10-13 is reflected in the data of Figures 14 and 15 where

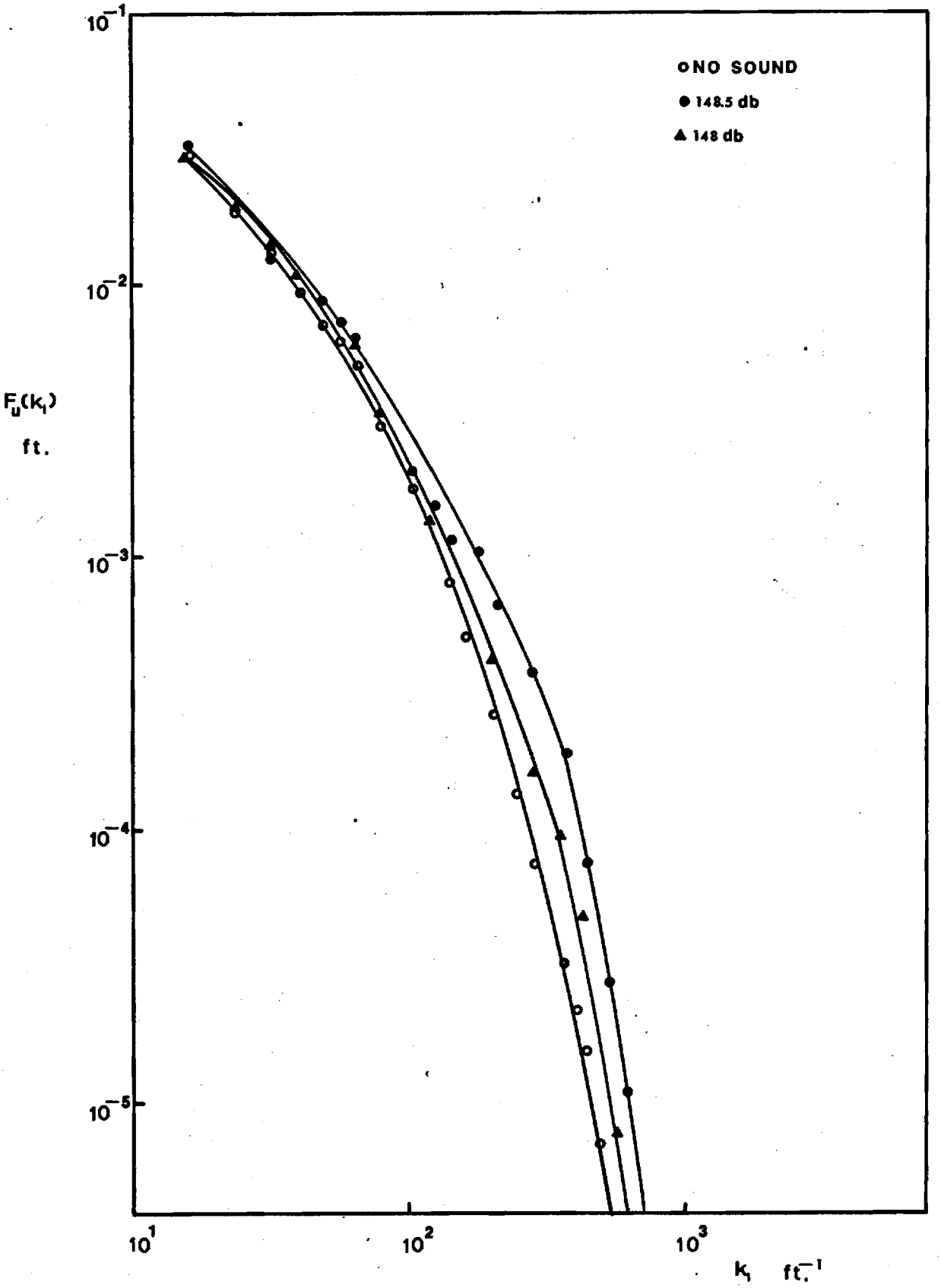

Figure 12. Normalized u' Spectra, Re = 40,000, $\frac{y}{R}$ = 0.0165, $\frac{X}{D}$ = 30.3.

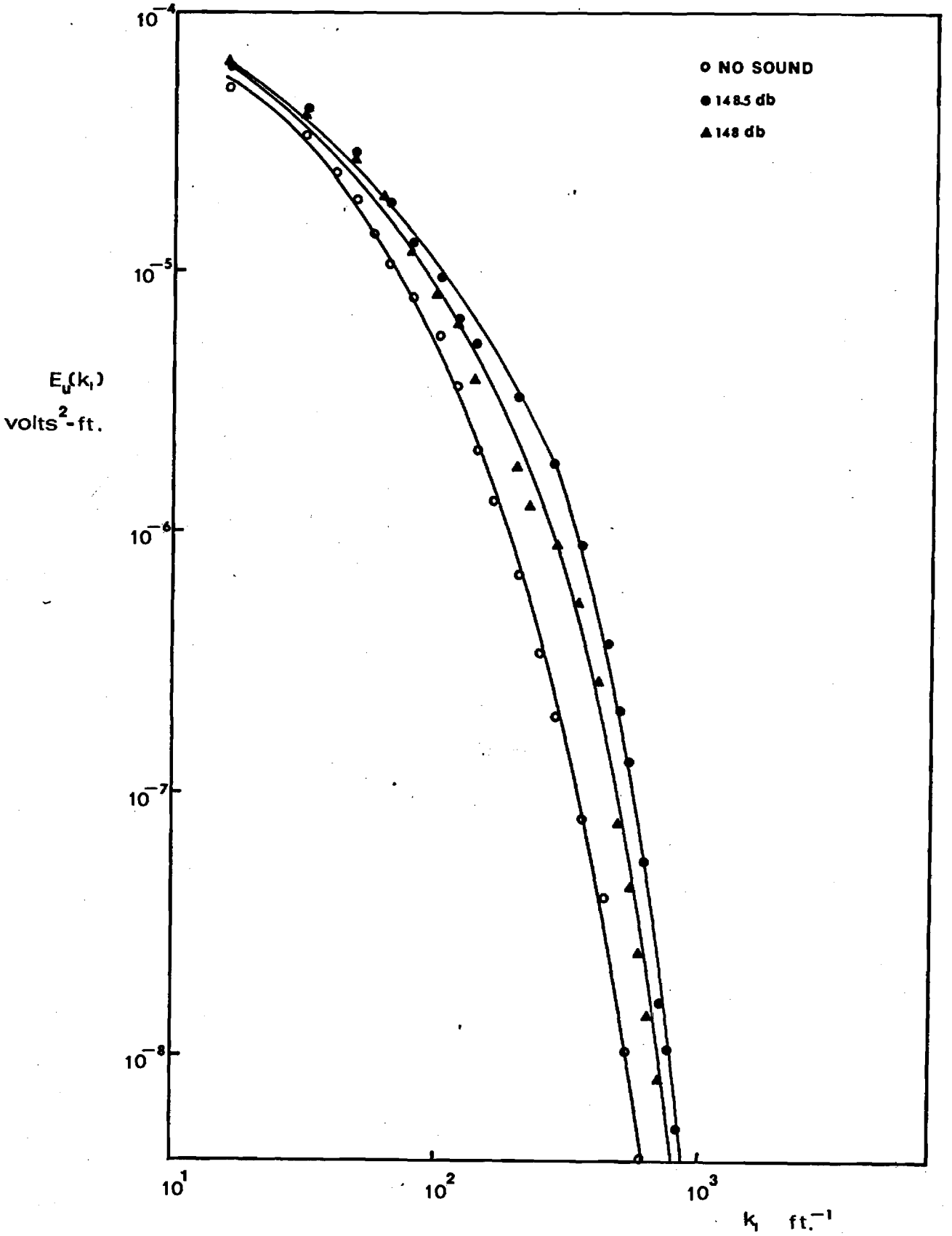

Figure 13. u' Spectra, Re = 40,000, $\frac{Y}{R}$ = 0.0165, $\frac{X}{D}$ = 30.3.

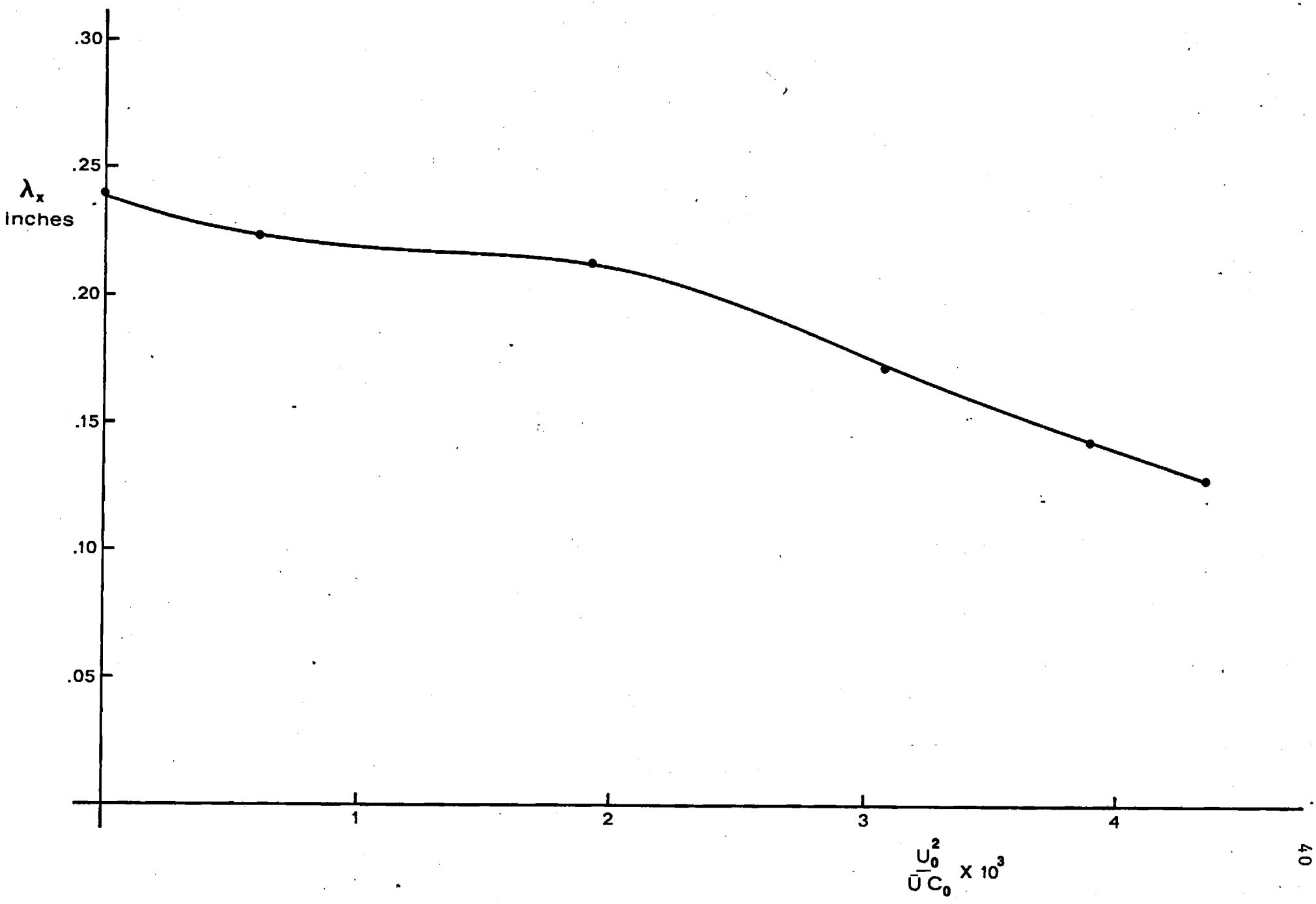

Figure 14. Longitudinal Microscale Re = 40,000, $\frac{Y}{R}$ = 0.0132, $\frac{X}{D}$ = 30.3.

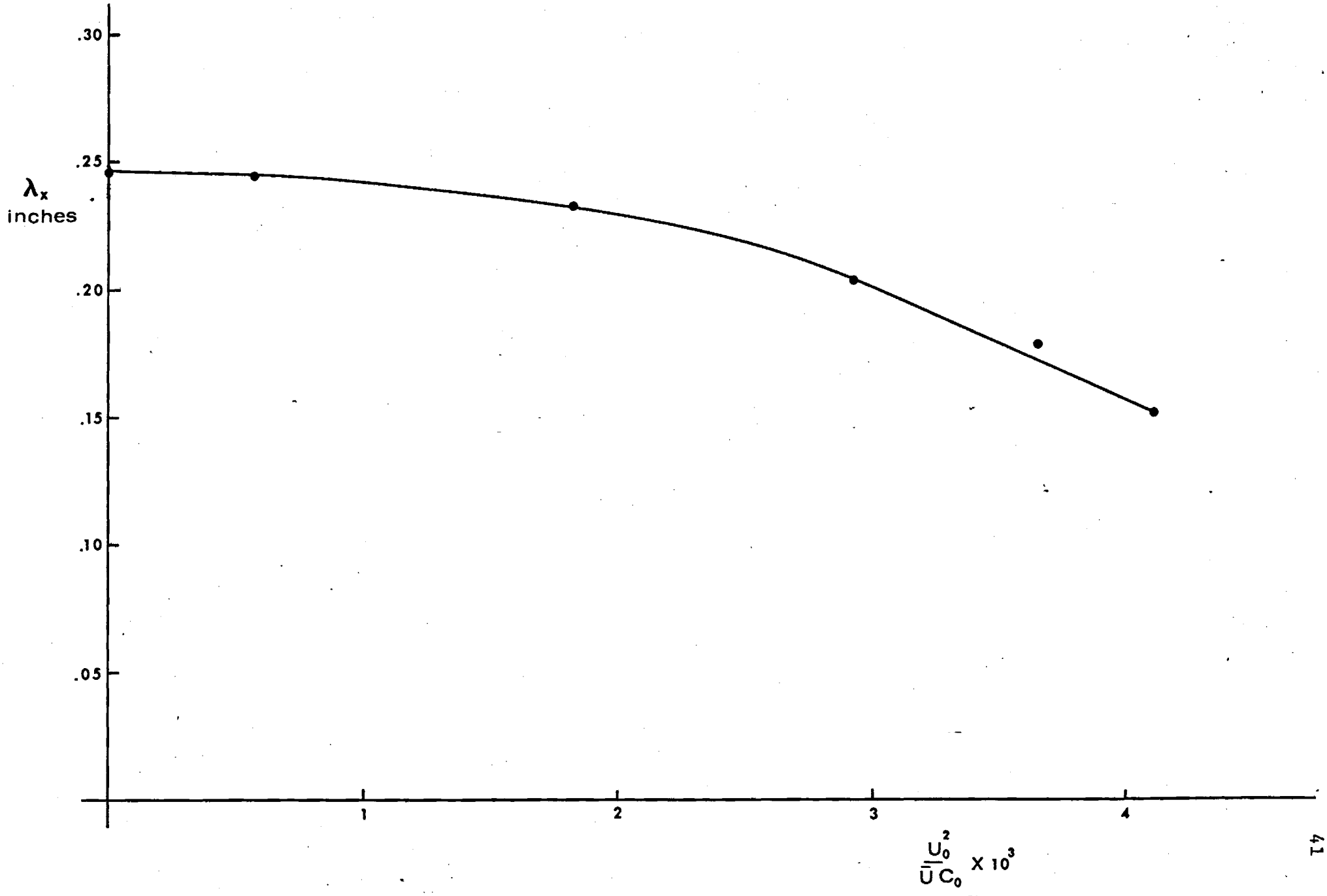

Figure 15. Longitudinal Microscale Re = 40,000, $\frac{Y}{R}$ = 0.0165, $\frac{X}{D}$ = 30.3.

the three largest values of $U_o^2/\bar{U}C_o$ are for sound pressure levels of 147.0 db, 148.0 db, and 148.5 db.

Conclusions in regard to effect of the resonant acoustic field on the longitudinal component of the turbulence are, that for sound pressure levels equal to and above 147.0 db a significant change in the spectra and microscale result. The effect is one of increased energy particularly in the high frequency (high wave number) range, and both the energy density and normalized energy density show increases at discrete frequencies of greater than one order of magnitude for a sound pressure level of 148.5 db.

Radial Component

Data for the radial component was taken for flow conditions that were identical to that reported previously for the longitudinal component. The normalized energy density and energy density data shown in Figures 16 and 17 are for a radial location of y = 0.04 inches. It may be seen that the normalized energy shows a major part of the energy increase in the spectrum over the no sound data to be predominantly at the high wave numbers. This again seems to indicate that a significant transfer of low frequency energy (specifically that at the resonant frequency) is occurring as a result of the interaction phenomenon. The magnitude of the change in the spectra (148.5 db compared to no sound values) is particularly striking in the high wave number data of both Figures 16 and 17. From Figure 17 two facts are evident. The first is that the total energy has increased due to the addition of the acoustic field (an obvious result), and the second is that while the total energy has increased the energy contained in the low frequency regions has not. The implication here again is that the energy transfer mechanism is from large to small scale structure.

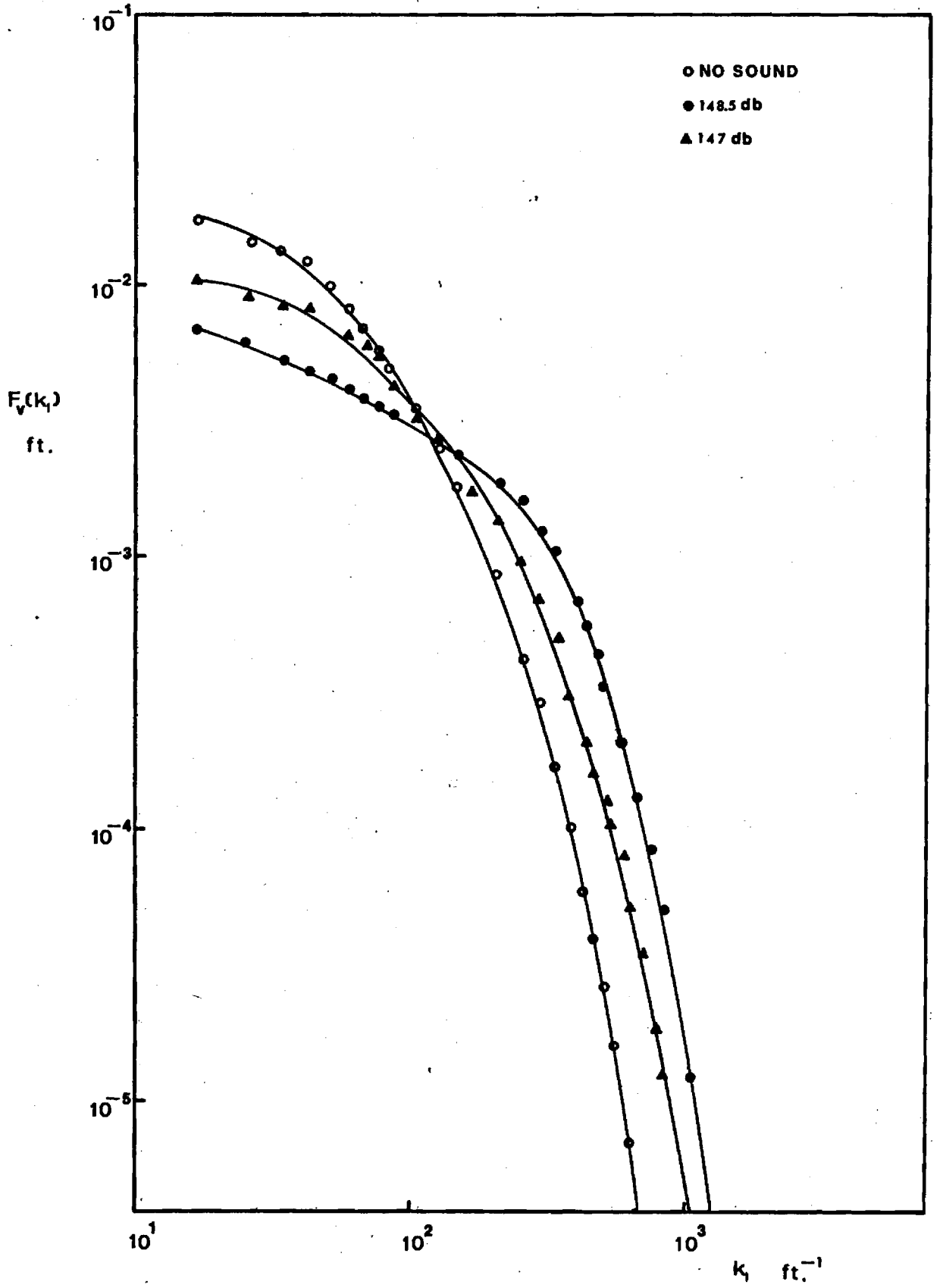

Figure 16. Normalized v'Spectra Re = 40,000, $\frac{Y}{R}$ = 0.0132, $\frac{X}{D}$ = 30.3.

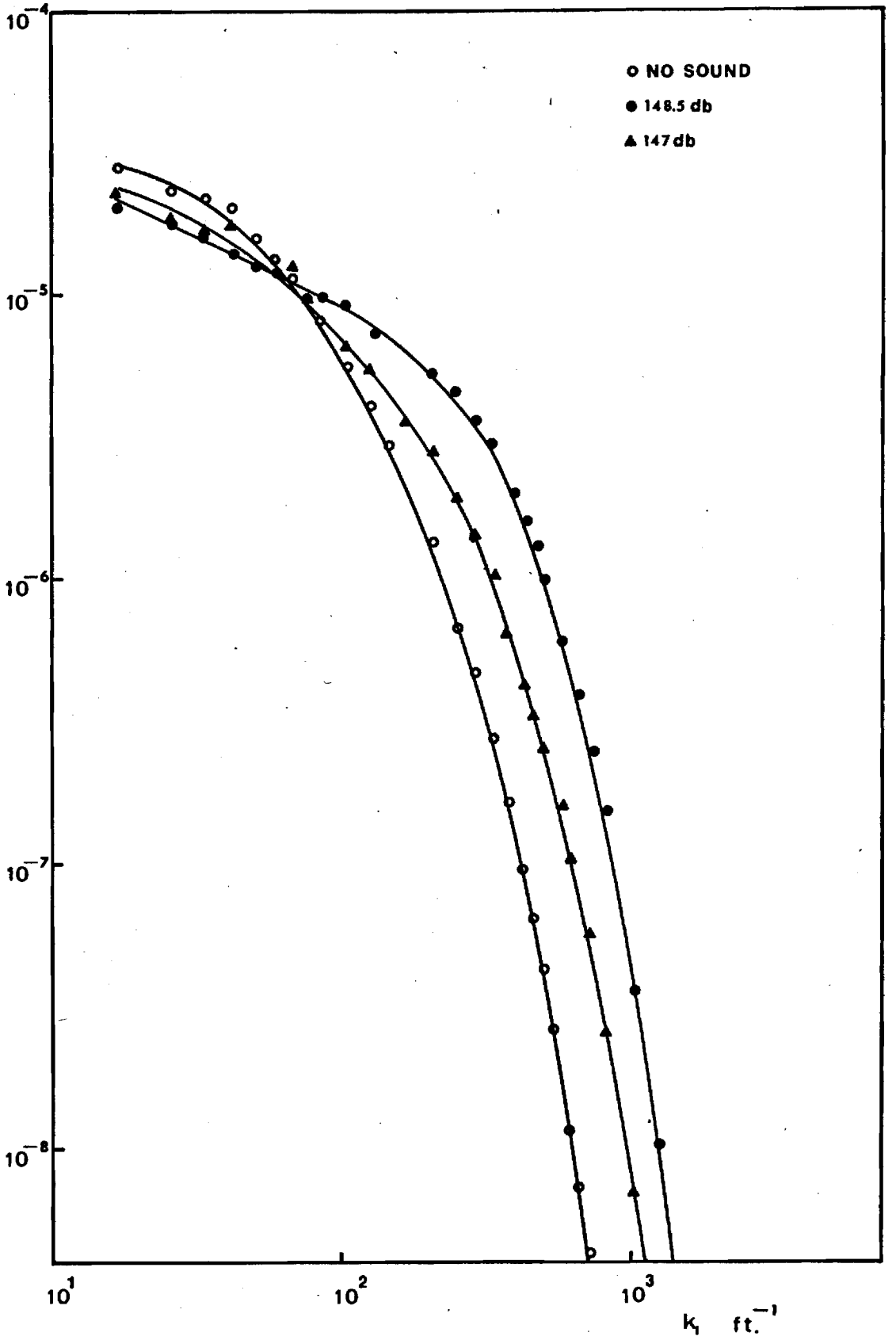

Figure 17. v'Spectra, Re = 40,000, $\frac{Y}{R}$ = 0.0132, $\frac{X}{D}$ = 30.3.

The data in Figures 18 and 19 show the effect of a change in radial location on the data in Figures 16 and 17. The trends are the same but the magnitude of the interaction effect is shown to have decreased for all values of sound pressure level considered. This is the result expected since preliminary data showed that it was very difficult to obtain a measurable effect at the intensities obtainable for distances from the wall greater than about 0.25 inches with other variables being the same.

By integration of the spectra of Figures 16 and 18 the lateral microscale λ_r was obtained, and is shown in Figures 20 and 21. The most significant effect of the acoustic field on this parameter is found for the radial location nearest the wall, namely y = 0.04 inches. Again the abscissa is $U_o^2/\bar{U}C_o$, and the lateral microscale for a sound pressure level of 148.5 db is about half of the corresponding no sound value. For y = 0.05 inches the reduction in size of the lateral microscale for a sound pressure level of 148.5 db is about 30 percent when compared to the no sound value.

Circumferential Component

As for the other two components, two radial positions were investigated for the circumferential component for various sound pressure levels ranging from 140.0 db to 148.5 db. In all cases the axial location was a velocity antinode (X/D = 30.3) and the Reynolds number was held constant at 40,000. Figures 22 and 23 illustrate the data for y = 0.04 inches and while there is certainly a significant effect, it does not appear that the circumferential component is affected as greatly as either the longitudinal or radial components. The interaction mechanism manifests itself in the now familiar increase in the energy of the high frequency region of the spectrum. The mechanism of energy transfer among eddies of various sizes is again being illustrated, and it may

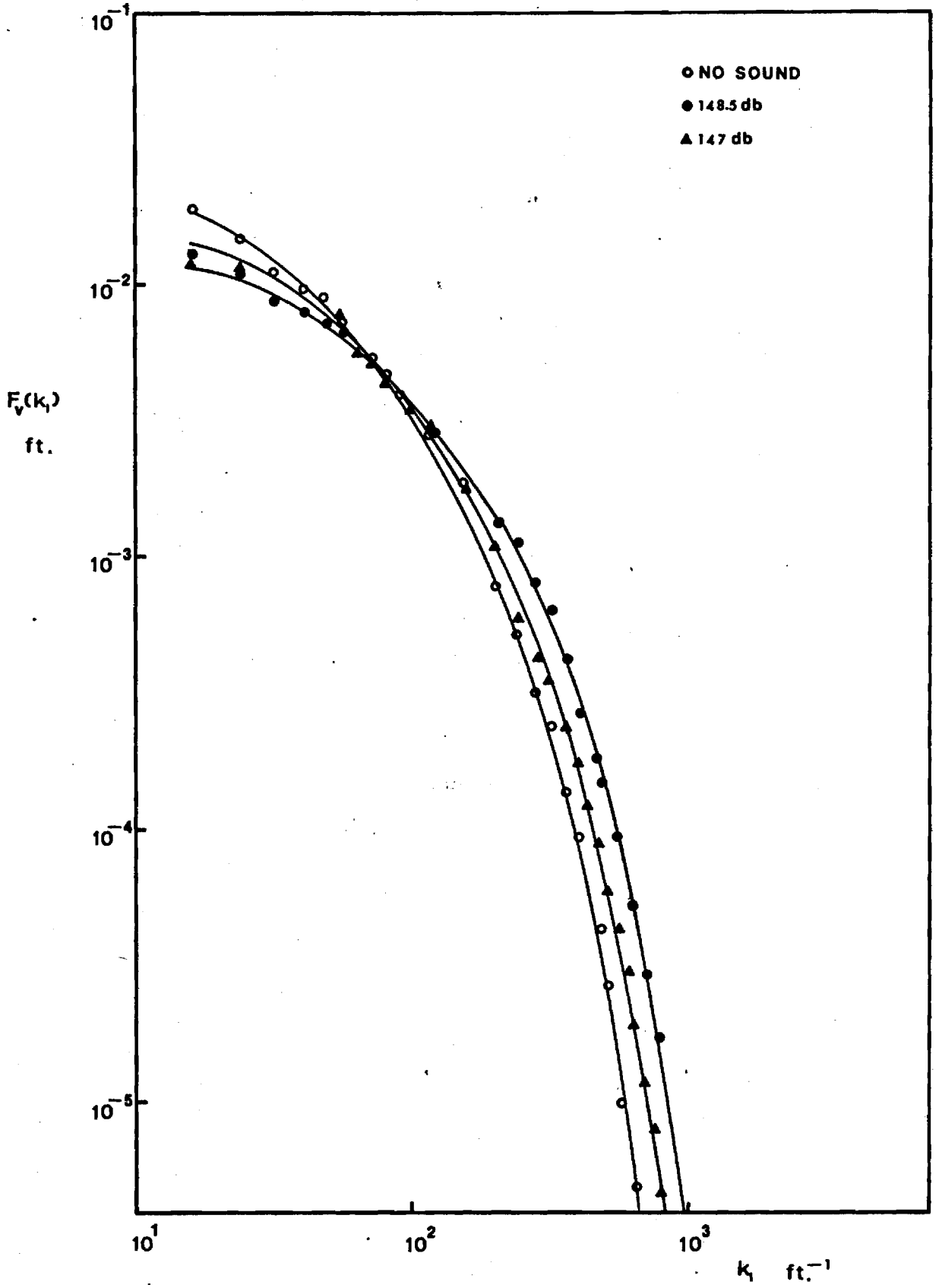

Figure 18. Normalized v'Spectra, Re = 40,000, $\frac{Y}{R}$ = 0.0165, $\frac{X}{D}$ = 30.3.

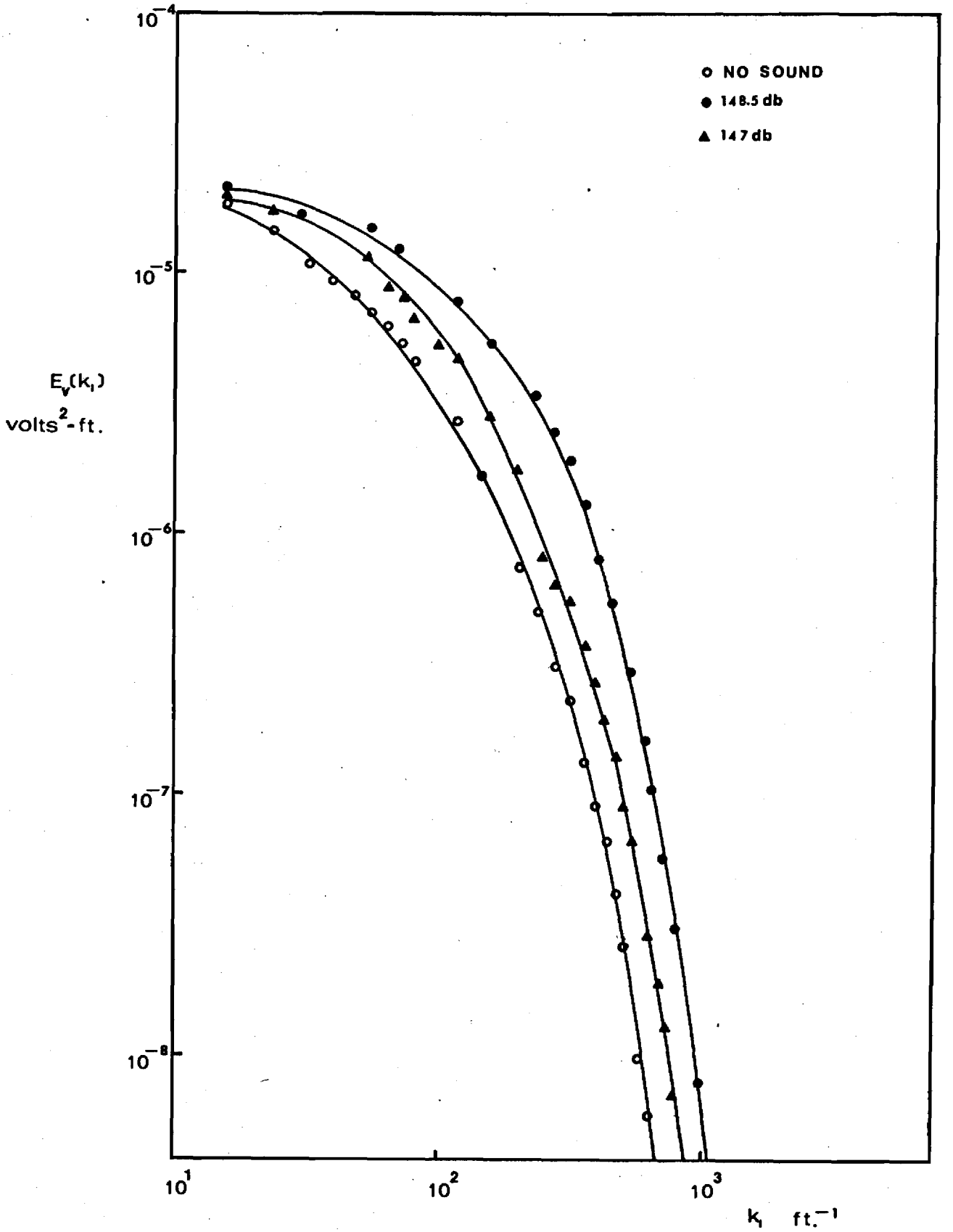

Figure 19. v' Spectra Re = 40,000, $\frac{y}{R}$ = 0.0165, $\frac{X}{D}$ = 30.3.

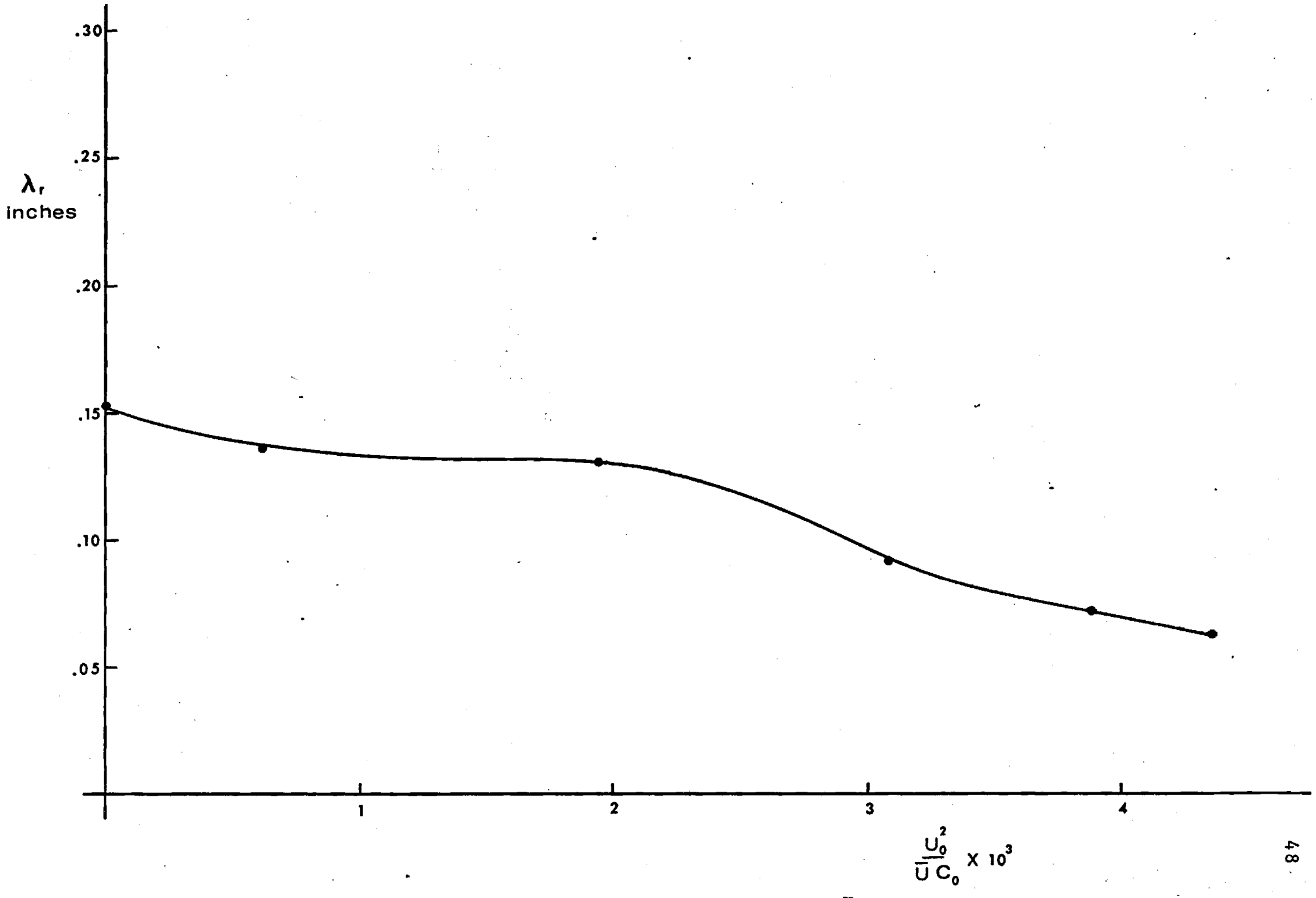

Figure 20. Lateral Microscale Re = 40,000, $\frac{Y}{R}$ = 0.0132, $\frac{X}{D}$ = 30.3.

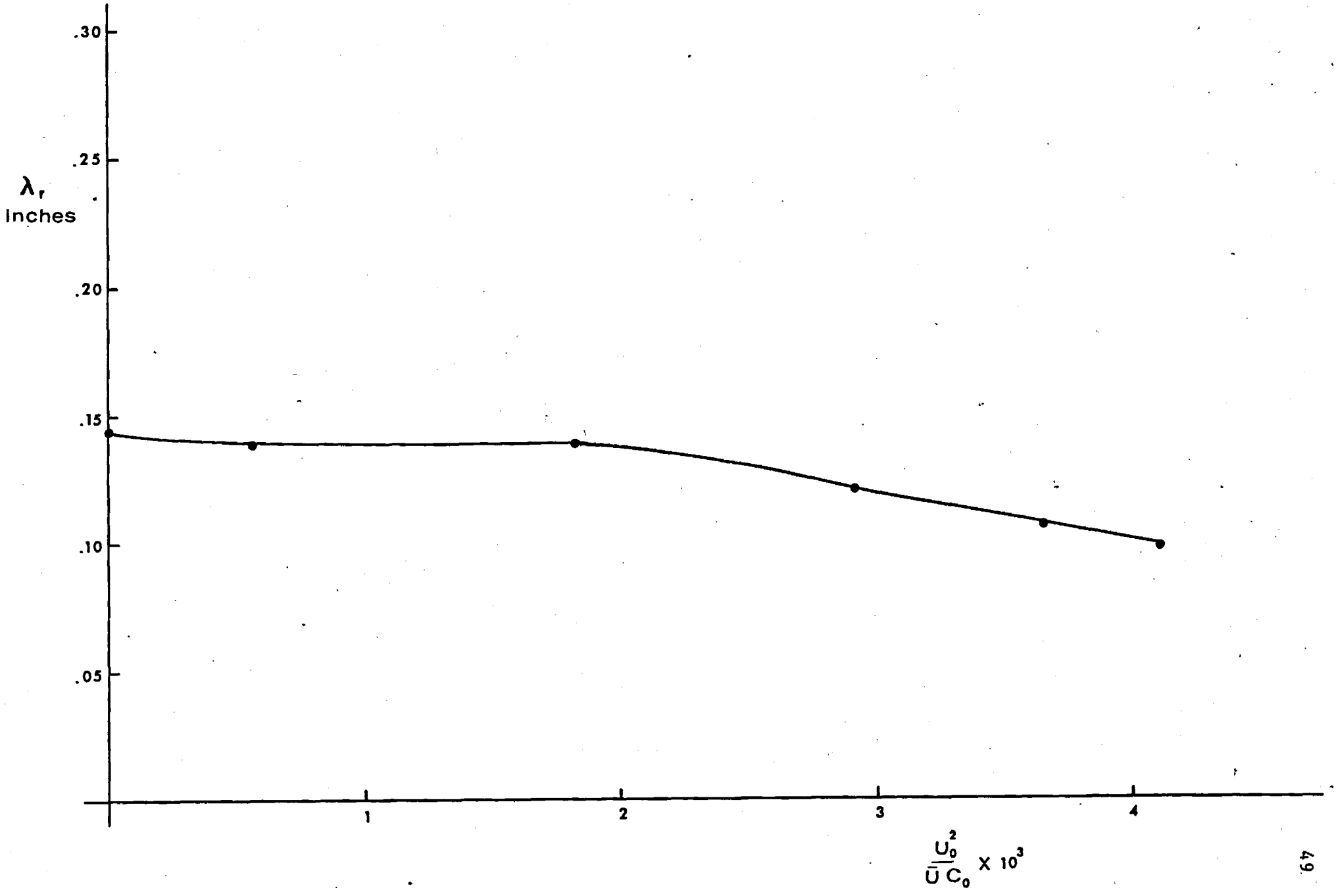

Figure 21. Lateral Microscale Re = 40,000, $\frac{Y}{R}$ = 0.0165, $\frac{X}{D}$ = 30.3.

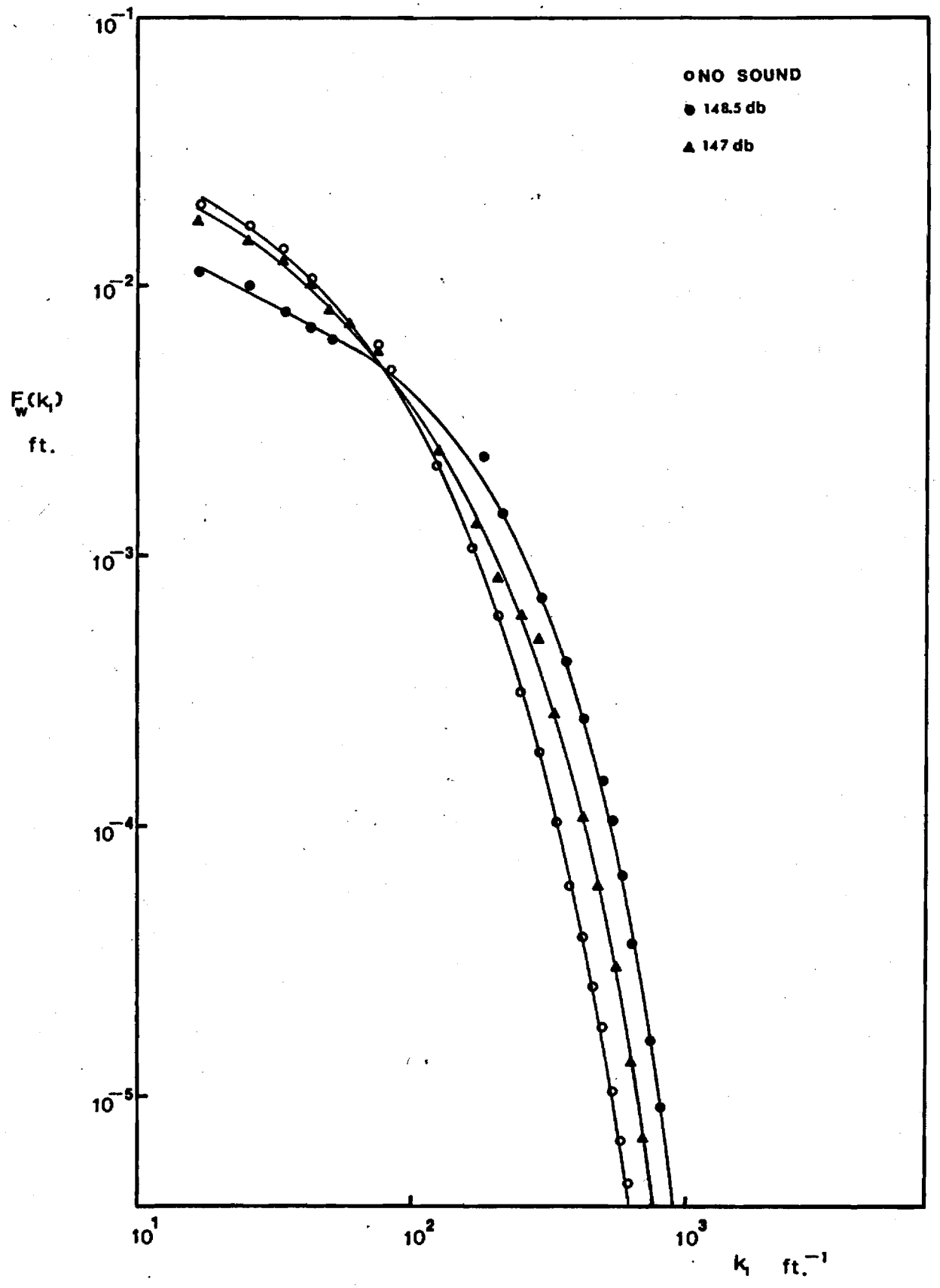

Figure 22. Normalized w' Spectra, Re = 40,000, $\frac{y}{R}$ = 0.0132, $\frac{X}{D}$ = 30.3.

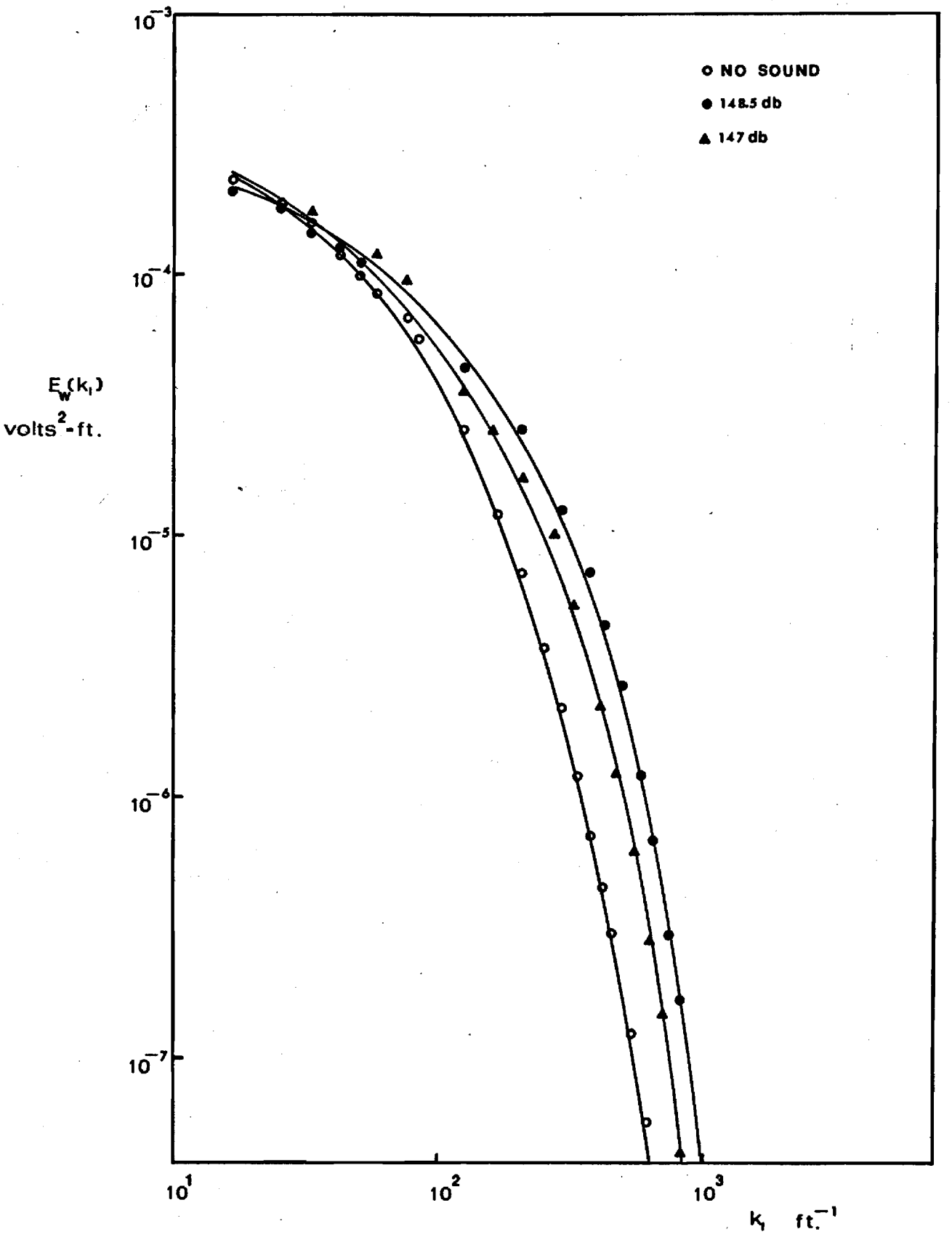

Figure 23. 'w' Spectra, Re = 40,000, $\frac{Y}{R}$ = 0.0132, $\frac{X}{D}$ = 30.3.

be assumed to be physically similiar in nature to that for the other components.

Figures 24 and 25 show very clearly how the interaction effect has become less severe as the radial location has been increased to 0.05 inches. It should be noted that there is virtually no change in the amount of energy contained in the low frequency end of the spectrum which suggests the likelihood that the energy of the acoustic field does not significantly affect frequencies below it (here about 110 Hz).

Flow Visualization Results

Figure 26 illustrates smoke being injected into the plexiglass test section from an injector at the bottom wall for a normal turbulent flow condition (no sound field superimposed upon the flow). The smoke immediately turns downstream and remains in the wall region at all times. (The bright area in the upper and lower left hand corner of each frame is due to reflections of the light source off of the test section). The smoke trace is continuous and regular in nature as it demonstrates the pathline for fluid particles. There was a slight normal velocity component at the wall (the injection velocity), and this was kept as small as possible consistent with the requirement that sufficient smoke was injected to make it visible.

Figure 27 is a series of photographs representing one complete acoustic cycle at 110 Hz at a sound pressure level of 144.5 db. The difference between these series of photographs and the no sound photographs is most clearly evident in more chaotic behavior of the smoke trace. The fact that the smoke now resides for the most part farther from the wall of the test section is due to the fact that as the flow at the wall is reversed due to the magnitude of the acoustic particle velocity, the smoke is being injected into a region of

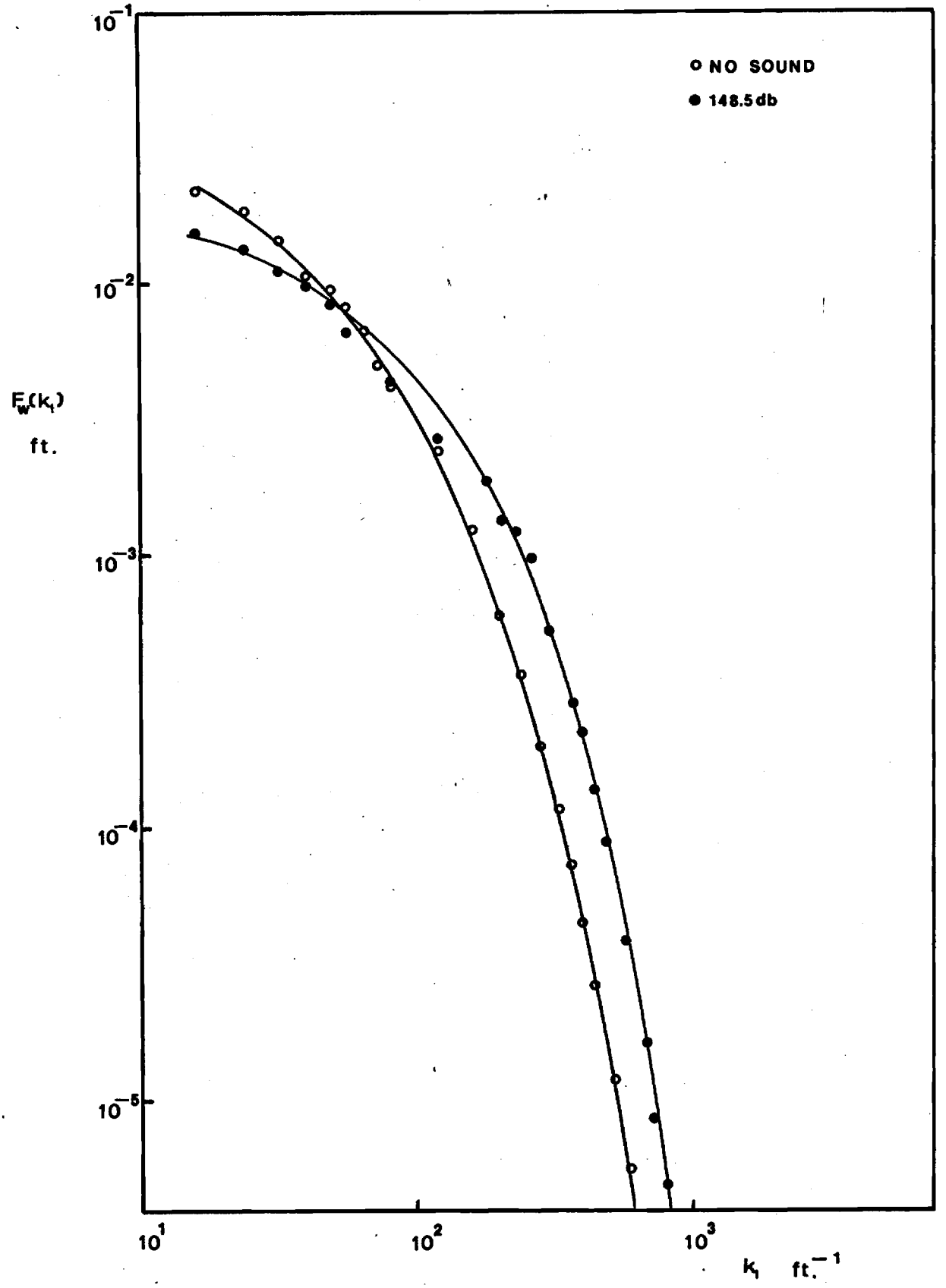

Figure 24. Normalized w' Spectra, Re = 40,000, $\frac{Y}{R}$ = 0.0165, $\frac{X}{D}$ = 30.3.

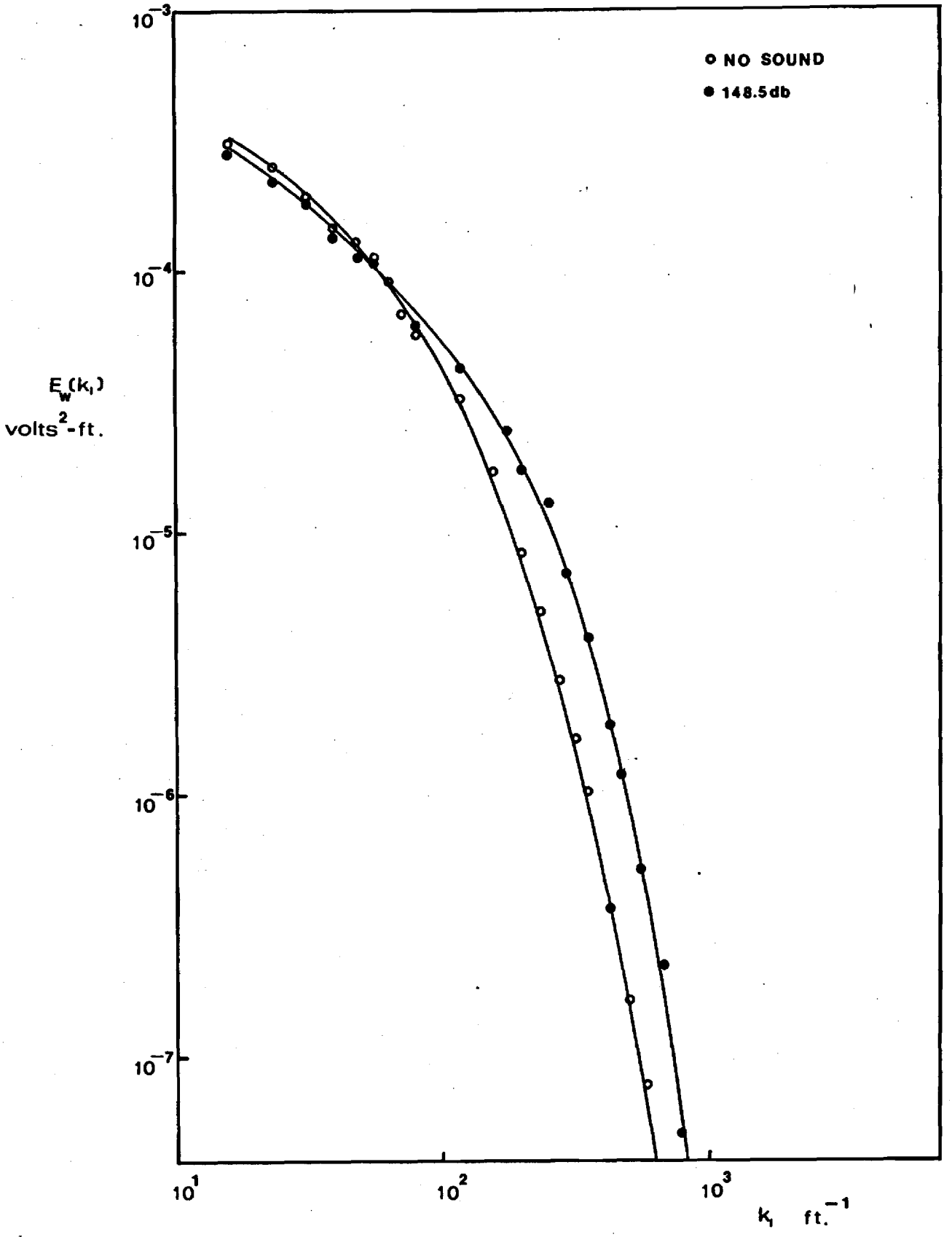

Figure 25. w' Spectra, Re = 40,000, $\frac{Y}{R}$ = 0.0165, $\frac{X}{D}$ = 30.3.

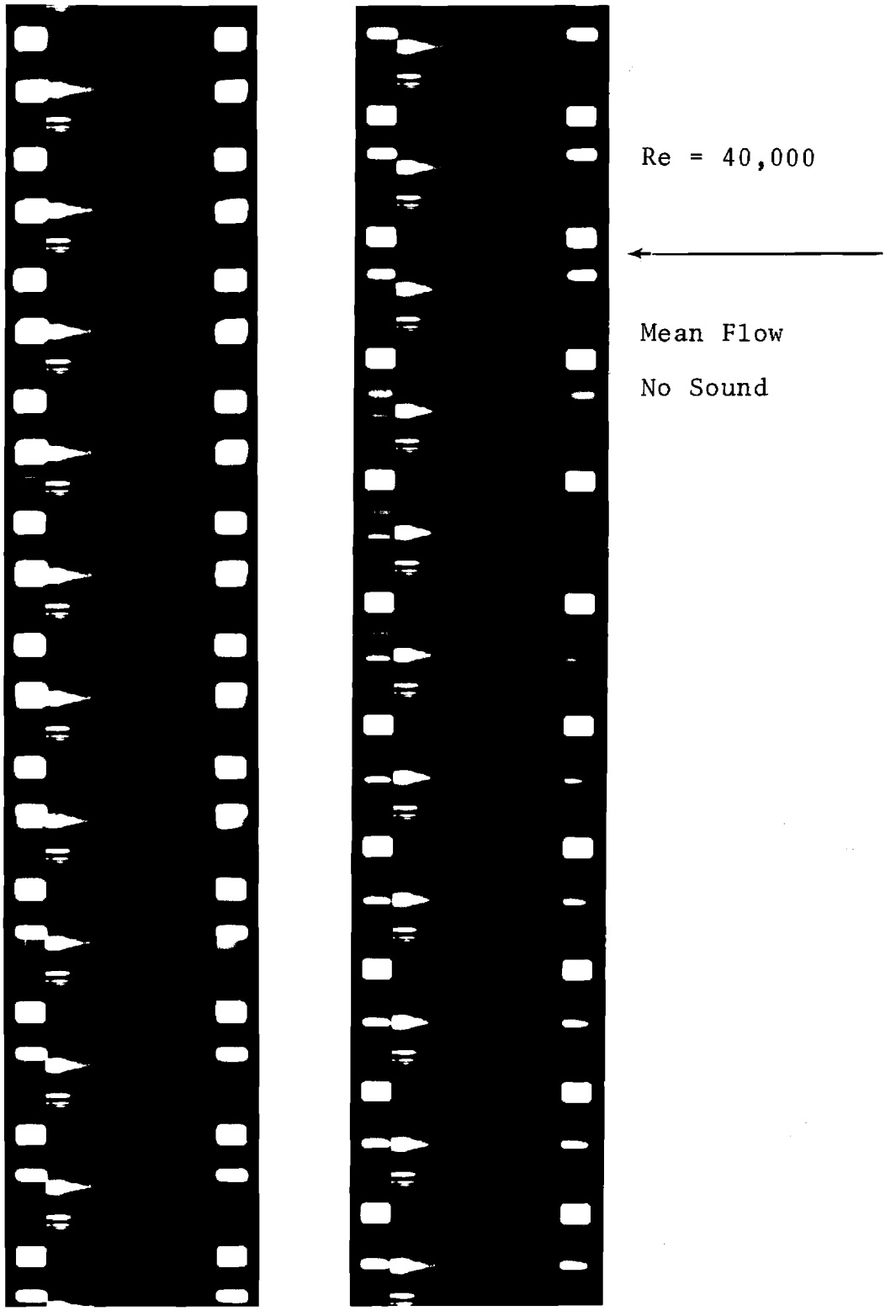

Figure 26.

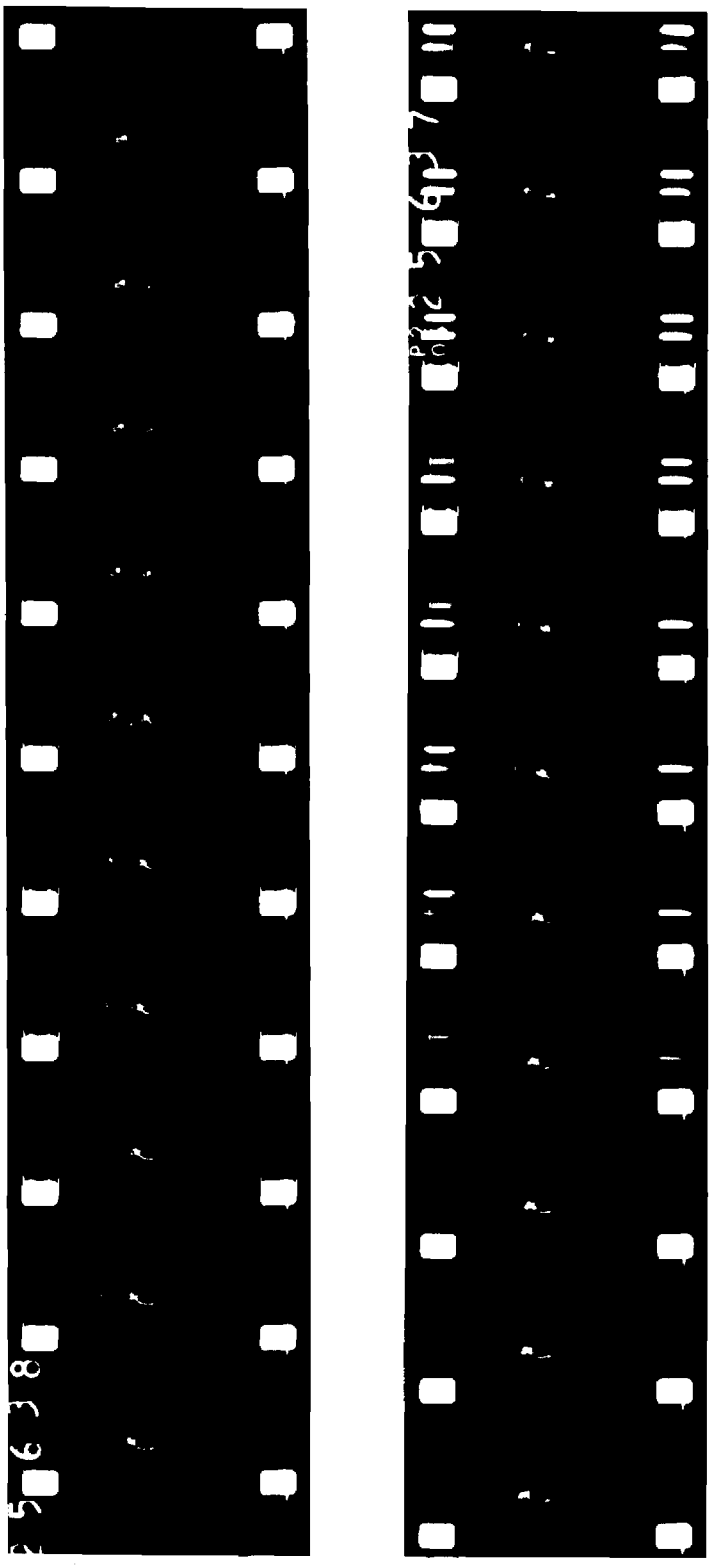

Re = 40,000

Mean Flow

SPL = 144.5 db

Figure 27.

virtually zero axial velocity. The inertia of the injected smoke carries it farther from the wall and as the acoustic field reverses in direction to assume the mean flow direction the smoke is then convected downstream. This type of behavior occurs in "bursts" characterized by the resonant frequency of the impressed acoustic oscillation. One very important point should be considered and that is in regard to flow reversal itself. In order to achieve clarity of the interaction process a considerable volume of smoke had to be interjected into the flow field. A consequence of this is that the injection velocity was large enough to physically blow the smoke past the region very close to the wall where the acoustic field would be expected to most dominate the mean flow. Based on this fact it was not possible to visualize smoke actually moving upstream against the mean flow. It is my belief that even though this was not visualized it is in fact a reality, particularly at high acoustic intensities.

Figure 28 is a series of photographs for a complete cycle for a sound pressure level of 148.5 db and a frequency of 110 Hz. The photographs were taken at a velocity antinode as indeed was all of the flow visualization data. Again the photographs illustrate a "burst" characterized by the resonant frequency. It is not possible to observe flow reversal at the wall for the reasons mentioned previously, but the fact that the acoustic field can effectively, neutralize the local mean flow velocity at points across the test section diameter accounts for the presence of the smoke far from the wall. The interaction phenomenon appears to be characterized by an energy input which results from a pulse generated in or near the wall layers. Thus as the distance from the wall is decreased both the visible and measurable effect (hot-wire measurements) diminished.

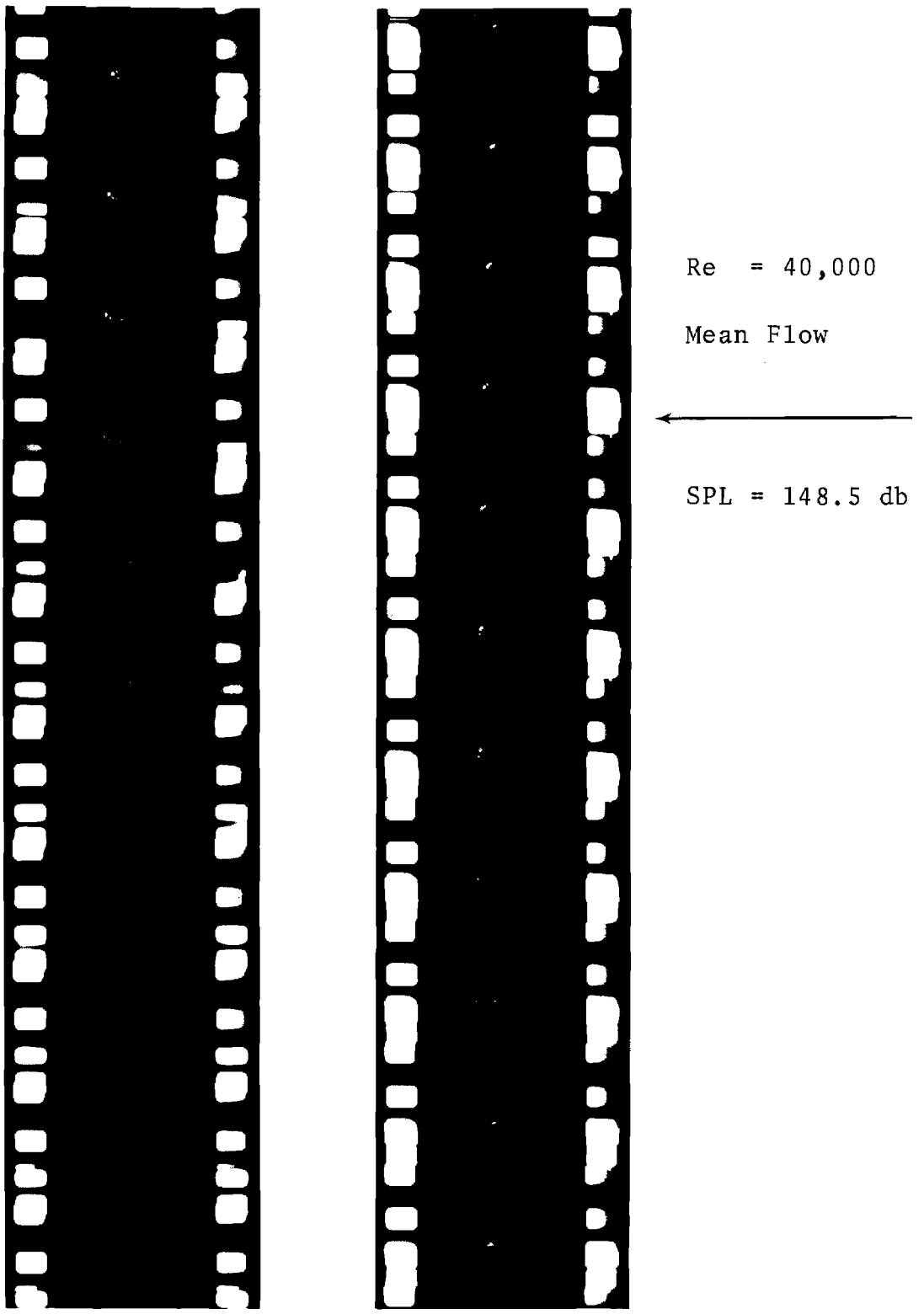

Figure 28.

XIII. Discussion of Interaction Model

The results of the flow visualization study do not seem to refute the model proposed in Reference 4. It still seems quite possible that a wall vortex is formed due to flow reversal, but due to the injection velocity of the smoke, the details of the interaction very close to the wall have been obscured. The fact that the flow reversal or neutralization of the local mean flow velocity still occurs near the wall where a significant mean flow velocity gradient exist, provides a mechanism for the transport of energy to other regions of the flow field. The shearing action can be observed to be taking place in the smoke traces of Figures 27 and 28.

It is still felt that the energy input whether manifested in the form of a wall vortex or not is still characterized by a burst of energy represented by the resonant frequency. The fact that the spectra of all of the turbulence components in the presence of the acoustic field illustrates that this energy appears at wave numbers above the resonant frequency means that a significant energy transfer has occured. It has occured from low frequency to high or from large eddy structure to small. It seems likely that the small scale eddy structure has increased energy when the acoustic field interacts with the flow. Thus smaller eddies are more able to withstand the viscous shearing effects. Thus we see that those eddies primarily considered to be responsible for dissipation have shown a reduction in average size when the sound field interacts with the normal flow. (See for example Figures 14, 15, 20 and 21).

XIV. Summary

It has been verified with both hot-wire anemoneter measurements and high speed photographs that a longitudinally resonant acoustic field of

sufficient intensity can significantly affect both the turbulent energy spectra and the turbulent structure. Preliminary spectrum measurements illustrated a need for moderate Reynolds numbers (this constraint was a result of the levels of acoustic input attainable) and a Reynolds number of 40,000 was selected. These preliminary results also demonstrated the desirability of making all measurements at a velocity antenode to realize the maximum effect, as well as specifying the radial locations to be employed namely y = 0.04 inches and y = 0.05 inches.

Final results were presented for three of the turbulence components with varying levels of acoustic input ranging from 140.0 db to 148.5 db. These results illustrated a significant effect of the sound field on all of the components and showed that the effect diminished with increasing distance from the test section wall. Photographs of the interaction phenomenon illustrated a significant change in the normal flow process and led to an acceptance of the plausibility of the arguments put forth corresponding to the flow model in Reference 4.